ms I

PWA FR-952
13 APRIL 1964

54p

Cat-03 X64 35769
Code 2A
NASA CR 56336

A STUDY OF PRESSURE PREDICTION METHODS FOR RADIAL FLOW IMPELLERS

FINAL REPORT

GPO PRICE $ _____

OTS PRICE(S) $ _____

Hard copy (HC) 3.00

Microfiche (MF) .50

FACILITY FORM 602

N65 16499 (ACCESSION NUMBER)	(THRU)
54 (PAGES)	1 (CODE)
CR 56336 (NASA CR OR TMX OR AD NUMBER)	01 (CATEGORY)

[redacted]

Pratt & Whitney Aircraft DIVISION OF UNITED AIRCRAFT CORPORATION

FLORIDA RESEARCH & DEVELOPMENT CENTER

PWA FR-952
13 APRIL 1964

A STUDY OF PRESSURE PREDICTION METHODS FOR RADIAL FLOW IMPELLERS

FINAL REPORT

[redacted]

Written By: W. C. Keathley and H. F. Due Approved By: C. R. Comolli

W. C. Keathley
Program Manager

H. F. Due
Senior Engineer

C. R. Comolli
Supervisor

Prepared Under
Contract NAS8-5442
For
George C. Marshall Space Flight Center
Huntsville, Alabama

Pratt & Whitney Aircraft DIVISION OF UNITED AIRCRAFT CORPORATION

FLORIDA RESEARCH & DEVELOPMENT CENTER

FOREWORD

The work presented in this report was conducted at Pratt & Whitney Aircraft's Florida Research and Development Center as part of a program sponsored by the George C. Marshall Space Flight Center of the National Aeronautics and Space Administration, Huntsville, Ala. under contract No. NAS8-5442.

The work was administered under the Flight Mechanics branch, Mr. Loren C. Gross, Program Manager NASA, and covered the period from June 1963 to March 1964.

TABLE OF CONTENTS

SECTION		PAGE
	LIST OF ILLUSTRATIONS	iv
	LIST OF SYMBOLS	v
	ABSTRACT	vi
I	INTRODUCTION	I-1
II	EXPERIMENTAL TEST APPARATUS AND EQUIPMENT	II-1
III	RESULTS OF EXPERIMENTAL PROGRAM	III-1
	A. General	III-1
	B. Static Pressure Distributions	III-1
	C. Torque Measurements	III-13
	D. Blade-To-Blade Pressure Fluctuations	III-15
IV	PRESSURE DISTRIBUTION PREDICTION METHODS	IV-1
	A. General	IV-1
	B. Radially Outflowing Fluid Passing a Rotating Smooth Face	IV-1
	C. Radially Inflowing Fluid Passing a Rotating Smooth Face	IV-2
	D. Shutoff Flow for Smooth Impellers	IV-2
	E. Bladed Disk Radially Outward Flow, Radially Inward Flow, or Shutoff Flow	IV-2
V	CONCLUSIONS	V-1
VI	REFERENCES	VI-1

LIST OF FIGURES

FIGURE	TITLE
I-1	Comparison of Prediction Methods with High Pressure Lox Pump Data
II-1	Pressure Distribution Test Apparatus
II-2	Test Rotors
II-3	Schematic of Flow Loop
II-4	Data Recording Equipment
III-1	Radial Pressure Distribution Rig Showing Direction of Flow
III-2	Head Rise vs Wheel Radius Squared for Smooth Disk Rotor - Radially Outward Flow
III-3	Effect of Ratio of Fluid Tangential Velocity at Impeller Tip with Flow Coefficient at Impeller Tip
III-4	C_u/u vs C_m/u for Radially Outward Flow on a Smooth Disk
III-5	Smooth Disk C_u/u at Shutoff Flow
III-6	Head Rise vs Wheel Radius Squared for Smooth Disk Rotor - Radially Inward Flow
III-7	Effect of Flow Coefficient at Impeller Tip on Vortex Mode
III-8	Effect of Ratio of Fluid Tangential Velocity to Wheel Tangential Velocity at Impeller Tip with Flow Coefficient at Impeller Tip
III-9	Radial Pressure Distribution for Bladed Impeller (Radially Outward Flow Direction)
III-10	Radial Pressure Distribution for Bladed Impeller (Radially Inward Flow Direction)
III-11	Radius Ratio vs Fluid Velocity Ratio (Radially Outward Flow)
III-12	Radius Ratio vs Fluid Velocity Ratio (Radially Inward Flow)
III-13	Fluid Angular Velocity Correlation (Outward or Inward Flow, T = 0.125)
III-14	T/S vs Fluid Velocity Ratio (Radially Outward Flow)
III-15	T/S vs Fluid Velocity Ratio (Radially Inward Flow)
III-16	Fluid Angular Velocity Correlation (Outward Flow)
III-17	Fluid Angular Velocity Correlation (Inward Flow)
III-18	Fluid Angular Velocity Correlation (Inward or Outward Flow, T = 0.250)
III-19	Fluid Angular Velocity Correlation (Effect of No. Blades, Outward Flow)
III-20	Fluid Angular Velocity Correlation (Effect of No. Blades, Inward Flow)
III-21	Fluid Angular Velocity Correlation (Inward or Outward Flow, Various No. of Blades)
III-22	Smooth Disk Torque Data
III-23	Bladed Disk Torque Data
III-24	Correlation of C_M with T/S
III-25	Oscillograph Analysis of Test No. 11.09 ω_B = 363 cps
III-26	Oscillograph Analysis of Test No. 4.08; ω_B = 1940 cps
III-27	Panoramic Wave Analysis of Test No. 11.09; ω_B = 363 cps, Scale = 0-50 psi
III-28	Panoramic Wave Analysis of Test No. 4.08; ω_B = 363 cps, Scale = 0-50 psi
III-29	Blade Pressure Loading

LIST OF SYMBOLS

Symbol	Nomenclature	Units
b	Thickness of disk or impeller	Inches
C	Radial clearance between impeller edge and end wall	Inches
C_A	Axial clearance between casing and impeller blade	Inches
C_m	Meridional velocity component or through flow velocity of fluid	ft/sec
C_M	Torque coefficient for two faces of disk defined as, $C_M = M/ 1/2\ \rho\omega^2 R_o^5$	
C_u	Tangential fluid velocity component	ft/sec
f	Friction coefficient from Moody	
f( )	Function of	
g	Acceleration due to gravity	ft/sec^2
H	Fluid piezometric head	Feet
K	Ratio of angular velocities	Dimensionless
M	Frictional Torque (moment)	ft-lb
n	Vortex exponent defined by $C_u R^n$	Constant
N	Shaft rotational speed	rpm
$___o$	Subscript, o, referring to the outer edge of the disk or impeller	
P	Absolute pressure	lb/ft^2
Q	Flow rate	gpm
R	Radius of disk or impeller	Feet
Rey	Reynolds number of disk, $Rey = \omega R^2/\upsilon$	
S	Axial distance between casing and impeller surface $(T + C_A)$	Inches
T	Blade height	Inches
u	Tangential impeller or disk velocity component	ft/sec
$__{1,2}$	Subscripts referring to radial location on disk	
β	Angular velocity of fluid (core rotation)	rad/sec
γ	Specific weight of fluid, ρg	lb/ft^3
υ	Kinematic viscosity	ft^2/sec
ρ	Mass density	$slugs/ft^3$
τ	Boundary shear stress	lb/ft^2
ϕ	Flow coefficient at impeller tip, C_m/u	
ω	Angular velocity of impeller	rad/sec
W_B	Blade passing frequency	cycles/sec

ABSTRACT

16499

This report presents the work performed under Contract NAS8-5442, "Pressure Prediction Methods for Low Flow Radial Impellers." The program consisted of experimental tests and analysis to derive an accurate method for predicting the pressure distribution along radial-bladed and smooth rotating disks operating with little or no meridional flow.

Using water as the test fluid, tests were conducted on a test apparatus with an 11-inch diameter rotor over a range of rotor-to-casing axial clearances from 0.125 to 0.040 inch. Flow coefficients from zero to 0.02 and speeds from 2000 to 8000 rpm were investigated. Five rotor configurations were studied: (1) twenty-four blades, 0.125 inches high, (2) twenty-four blades, 0.250 inch high, (3) twelve blades, 0.125 inch high, (4) six blades, 0.125 inch high, and (5) a smooth disk.

Pressure data at several radial stations, torque data, and high-frequency blade-to-blade pressure data were taken at various flows and speeds for the specified configurations. Methods were derived from the data to enable a more accurate prediction of pressure distribution than have previously been available. A comparison of the applicable prediction methods with experimental data from an existing high pressure liquid oxygen pump is presented.

Author

SECTION I
INTRODUCTION

Axial thrust unbalance of the pump rotor was a major problem area encountered in tests of high pressure hydrogen and oxygen centrifugal turbopumps conducted at the Pratt & Whitney Aircraft Florida Research and Development Center. This problem developed because of the inaccuracy of available methods for predicting the distribution of pressure and the resulting thrust loads for the low-flow rear faces of the impellers.

Pressure distribution and thrust balance of rotating machinery is not a new subject. One of the first papers to appear in the literature was one by A. J. Stepanoff in 1932 (Reference 1). In his paper, Stepanoff presented an equation relating to pressure distribution along an impeller back face where the meridional flow was considered to be zero. A. J. Acosta reported in Reference 4 a study where he compared experimental data with a two-dimensional analysis for flow through an enclosed vane passage operating at relatively low flow rates.

Unfortunately, the results discussed by these and other investigators are not directly applicable to high pressure turbopumps. Stepanoff's study was conducted for flow coefficients of zero, or in other words for no meridional flow. The high pressure pump rolling element bearings are cooled by the particular propellant being pumped. Since this coolant is supplied from the rear faces of the impellers, there is a resultant flow across the impeller and, therefore, the impellers do not operate at zero flow coefficient. Acosta analyzed and tested double shrouded vanes; but this type of vane is impractical for high speed rotors from a structural standpoint.

The high pressure liquid hydrogen pump that has been tested at the Florida Research and Development Center was designed assuming the back vane pressure distribution would develop according to Stepanoff's prediction method. The thrust on the back face of the second stage was predicted at 350,000 pounds. Measurements taken during early tests indicated an actual thrust load of 315,000 pounds. This 35,000-lb deviation in thrust, coupled with a similar inaccurate prediction of the thrust on the back face of the 1st-stage impeller, resulted in a change in the net rotor thrust that overpowered the thrust balance piston and caused pump failure. The pump was modified to reduce the thrust unbalance and the problem eventually corrected. But it was obvious that in applications where the pressure-area product is high, more accurate prediction methods are necessary. The subject program, the results of which are reported herein, was conducted to fulfill this goal.

The program conducted under Contract NAS8-5442 included the following items:

1. An experimental test program to determine the effect of axial clearance, blade height, number of blades, flow direction, flow magnitude, and rotor speed.
2. Analysis of the data and the formulation of an accurate prediction method.

A test apparatus was designed to accomplish the various facets of the test program and a test facility was adapted so that the tests could be conducted using water as the test fluid rather than a cryogenic fluid. To establish the basic trends for an incompressible fluid, water was chosen in this initial phase because of its economy and ease of handling. A range of small but finite flows was chosen for the test program since

most pumps operate with a small leakage flow along the backface (or balancing face) of the impeller. A flow coefficient of 0.02 was chosen as the upper limit.

Experimental data were obtained for smooth and bladed disks with axial clearances from 0.125 to 0.020 inch, blade heights of 0.125 and 0.250 inch, number of blades of 24, 12, and 6, and for radially inward and radially outward flow directions.

Torque data and high frequency pressure oscillation data were taken as additional means to study the flow on smooth and bladed rotating disks.

The pressure prediction method derived in this program was applied to a set of high pressure liquid oxygen pump data and the comparison showed remarkably good agreement. For the particular cases compared it was found that the derived method was 1 to 3.5% lower than the actual test data while Stepanoff's method predicted values 14 to 17% lower than the actual data. These comparisons are shown in figure I-1.

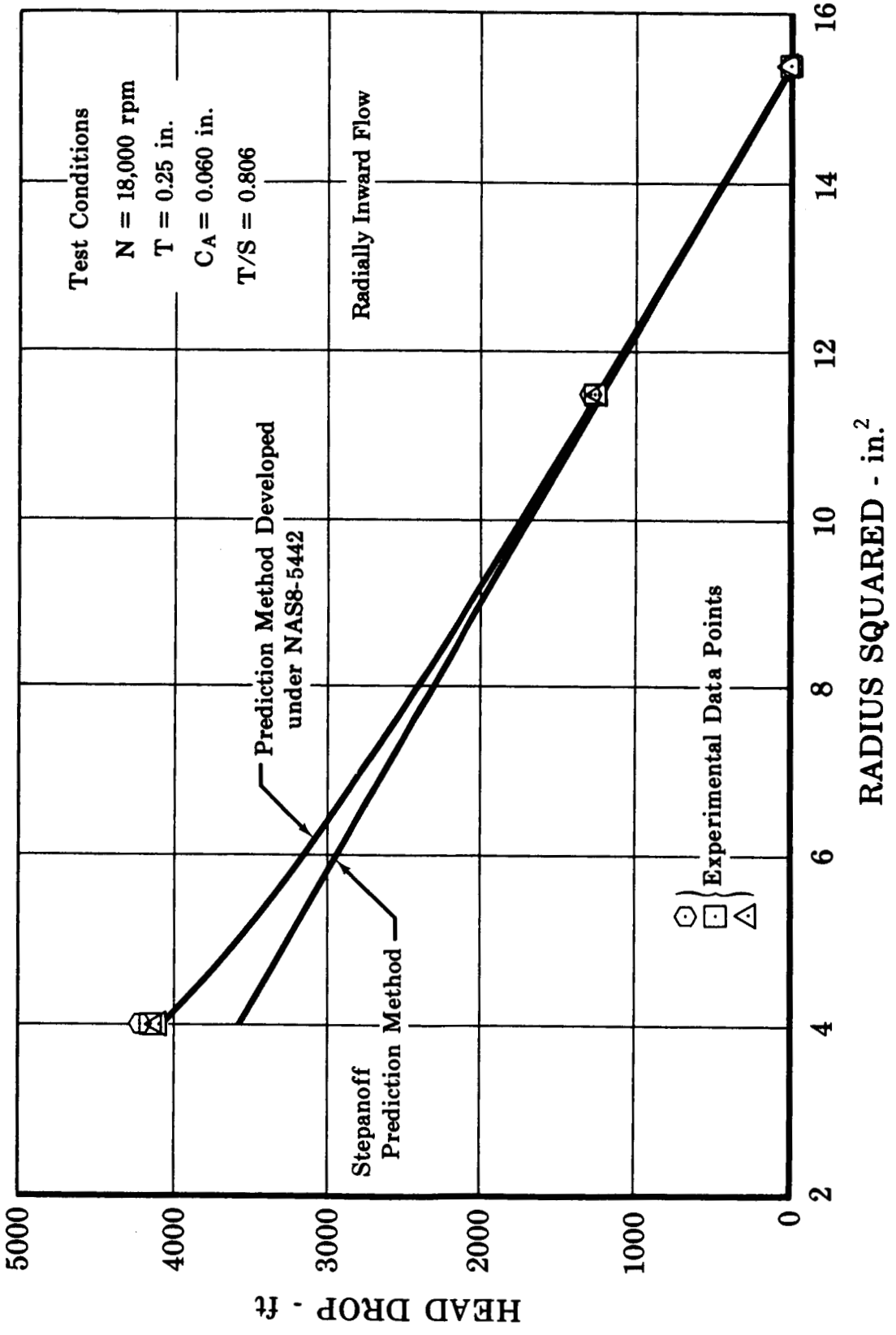

FD 7813

Figure I-1. Comparison of Prediction Methods with High Pressure Lox Pump Data

SECTION II
EXPERIMENTAL TEST APPARATUS AND EQUIPMENT

The test apparatus used in this study is shown in figure II-1. The apparatus was designed so that it could be easily adapted to different rotor and clearance configurations. The housings were purposely made much thicker than required by stress considerations to minimize axial deflection caused by pressure loading. The rotor was suspended by two grease-packed ball bearings that were loaded in the drive shaft direction. During a test run the net thrust load on the rotor was maintained in the drive shaft direction by means of an externally pressurized purge cavity located between the drive unit and the bearing housing to prevent shifting of the rotor and changing of the preset clearance. Figure II-2 shows photographs of two of the rotors and a dimensional sketch of the unbladed rotor. All of the rotors were fabricated using AMS 6260 steel and were coated with a lacquered graphite protective material, since AMS 6260 is not corrosion resistant. Three sets of shims were used to obtain the various clearance ranges required by the experimental program.

A schematic of the flow loop is shown in figure II-3. Water, which was the only test fluid used in this test program, was contained in a 5000-gal portable tank trailer. A pump was used to supply flow to the test apparatus and maintain the inlet pressure. The water was recirculated from the trailer through the boost pump, filter, turbine flowmeter, test apparatus, remotely controlled discharge valve, and returned to the trailer. The temperature of the water was measured with a copper-constantan thermocouple at the inlet to the test apparatus and also at eight other radial locations corresponding to each static pressure measurement.

The drive system consisted of a 1500-hp electric motor coupled with a Dynamatic clutch and an electronic speed controller. A gearbox and torque meter are included in the drive system. This system is shown schematically in figure II-3.

Most of the test data were taken in digital form using a high speed data recording system (figure I-4), which permits all instrumentation channels to be recorded every 14.5 milliseconds. There were 50 channels on the test apparatus, each of which was recorded 75 times per second. The test data were obtained as averages for each channel over a 2 second time interval.

The high frequency blade-to-blade pressure oscillation data were taken using a frequency-modulated tape unit so as to be available for analysis after a test run was completed.

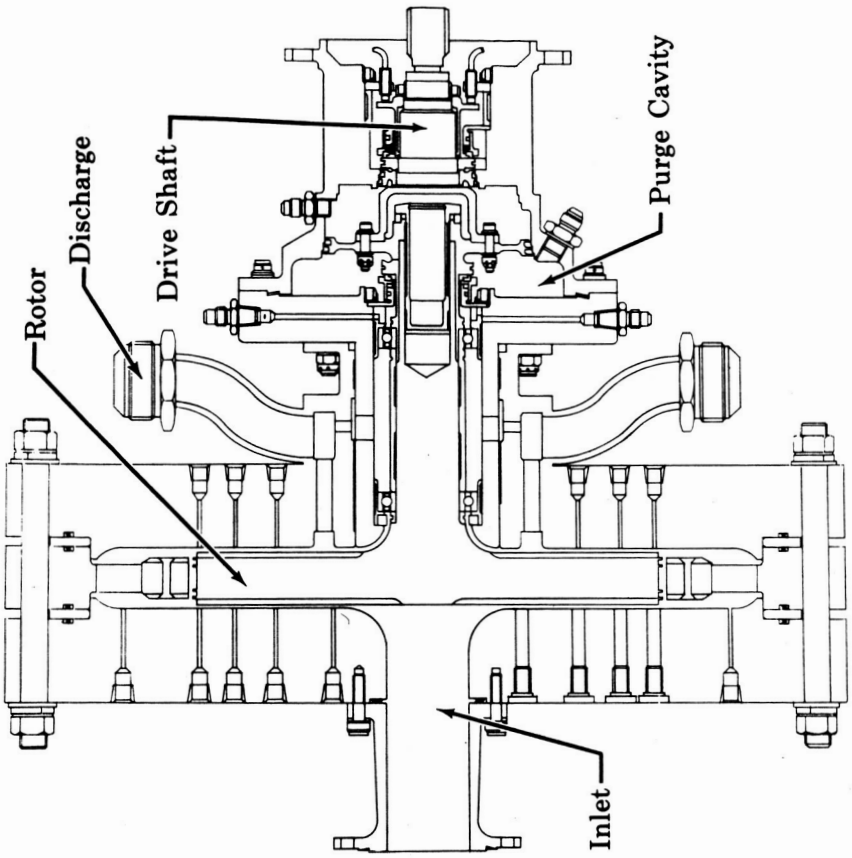

FD 7565

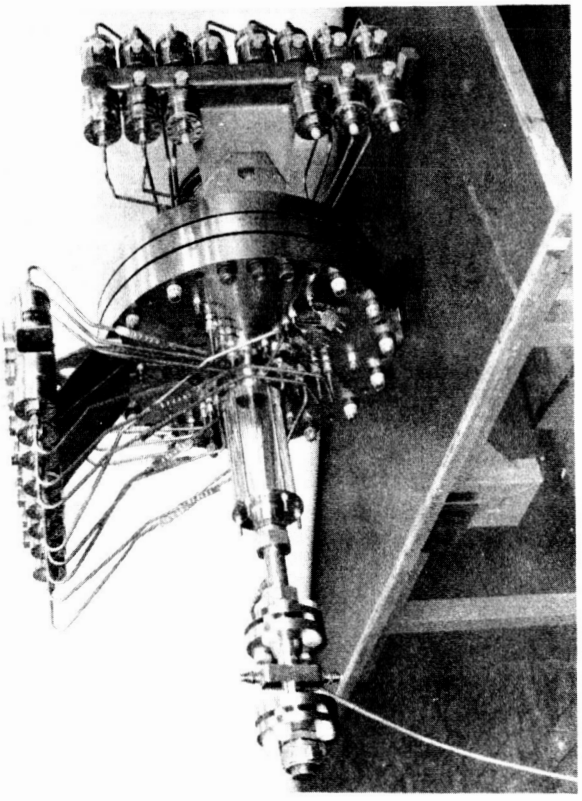

Test Apparatus with Pressure Transducer Lines Installed

Figure II-1. Pressure Distribution Test Apparatus

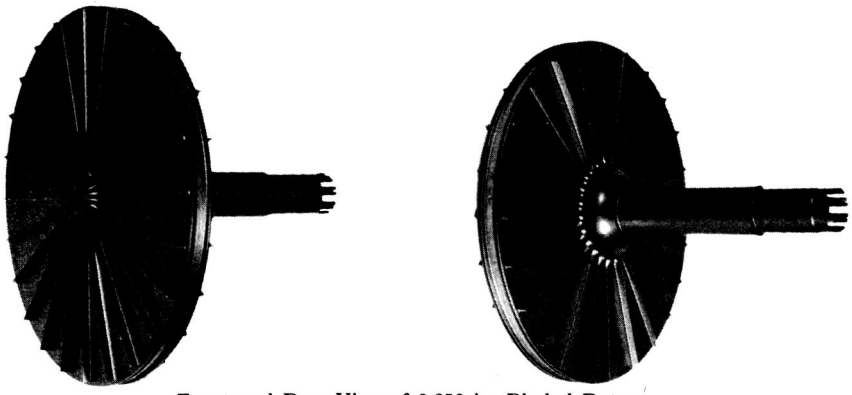

Front and Rear View of 0.250-in. Bladed Rotor

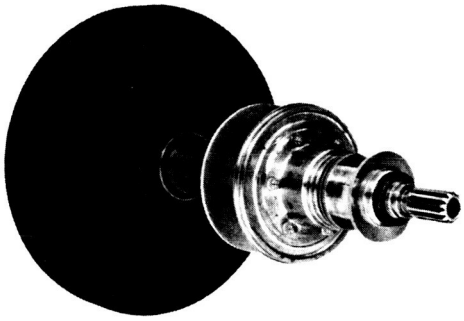

Assembly of Unbladed Rotor

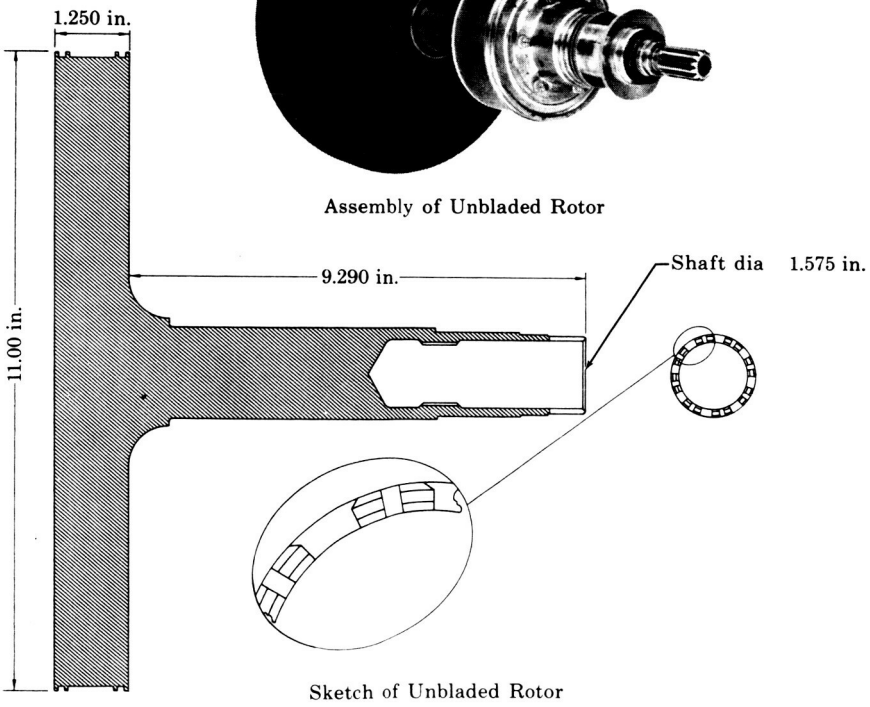

Sketch of Unbladed Rotor

Figure II-2. Test Rotors FD 7566A

FD 7563

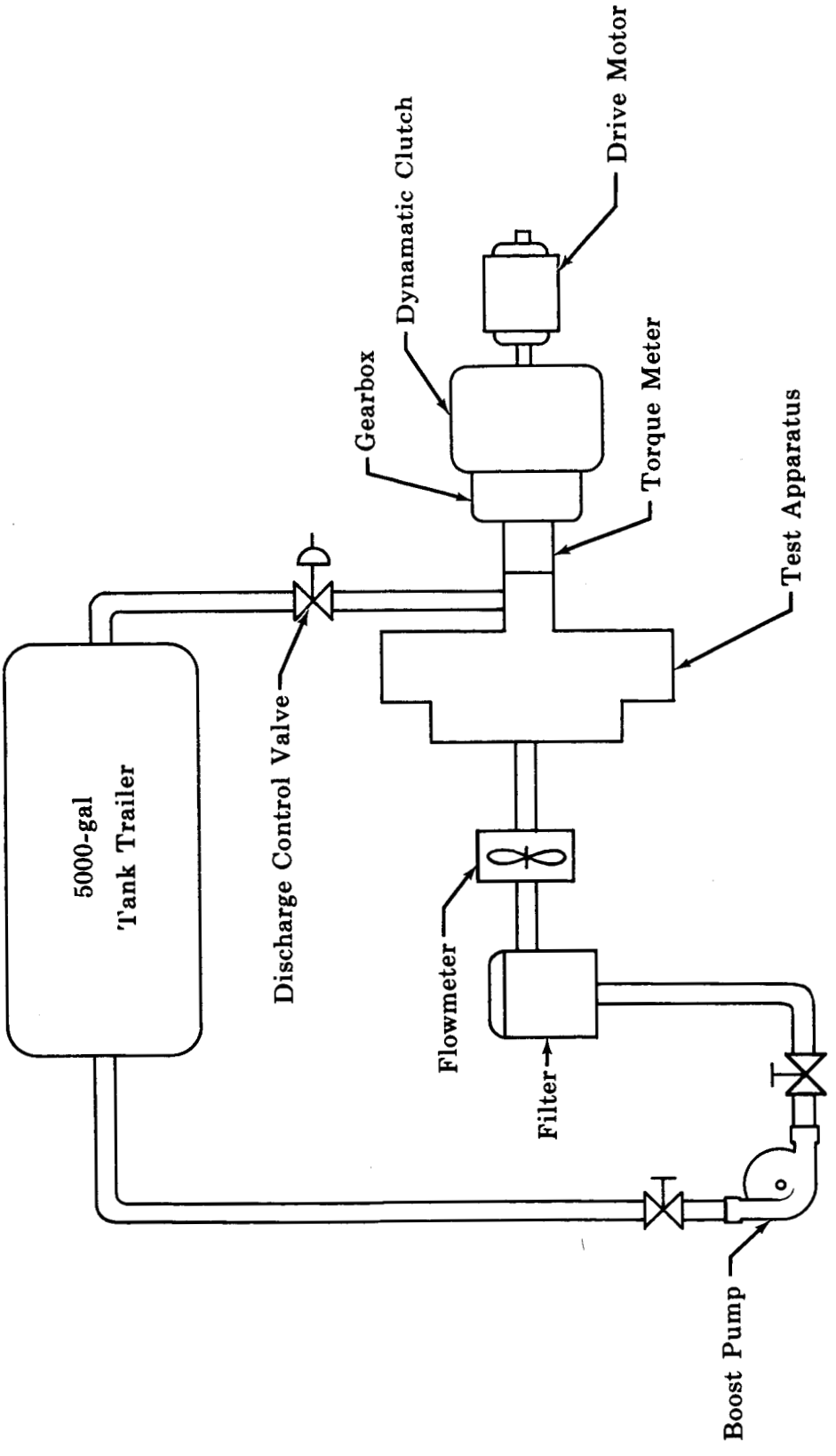

Figure II-3. Schematic of Flow Loop

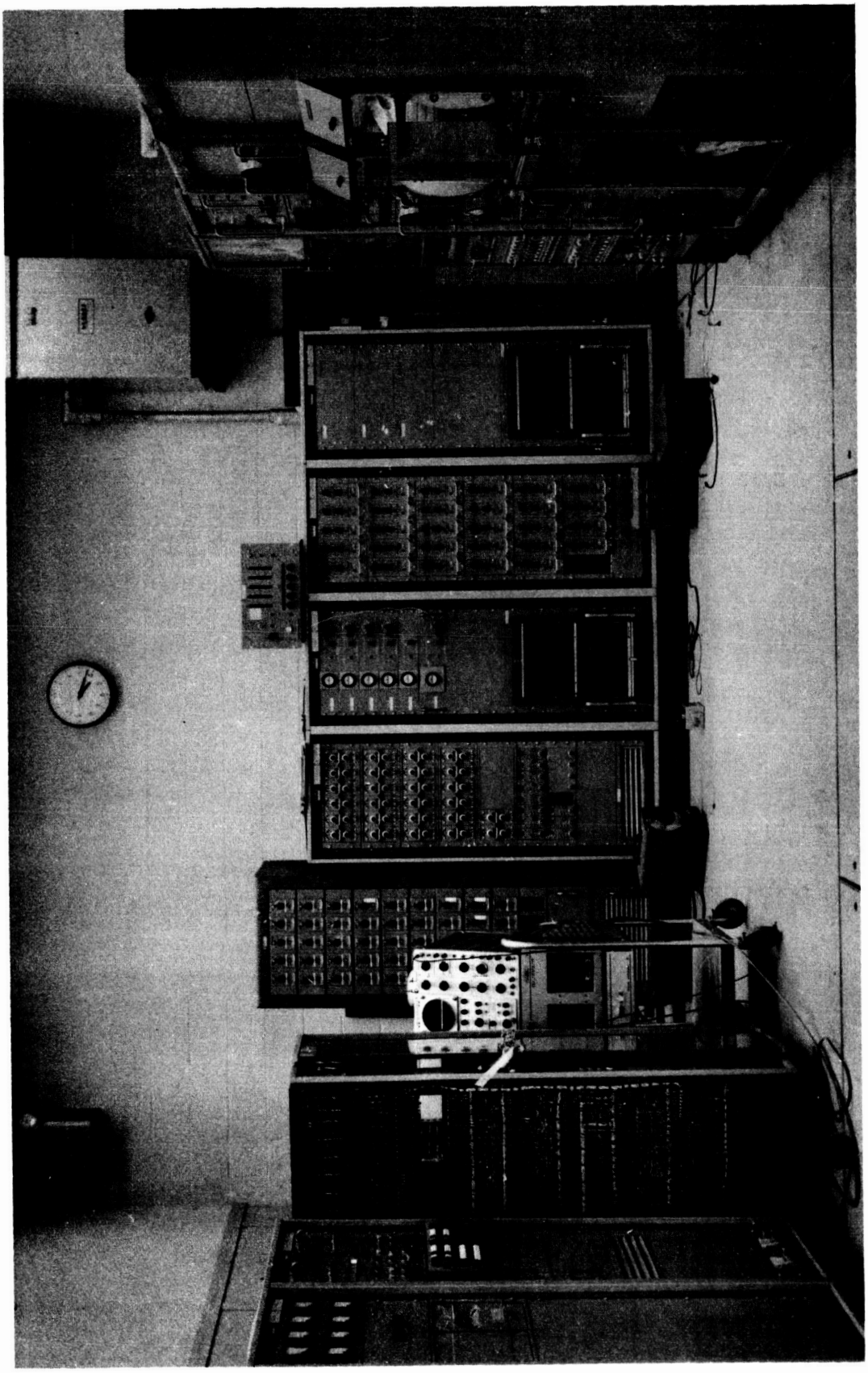

FC 3890

Figure II-4. Data Recording Equipment

SECTION III
RESULTS OF EXPERIMENTAL PROGRAM

A. GENERAL

The experimental program was planned to provide the maximum amount of information related to the distribution of pressure created by low-flow pumping surfaces of various configurations. As shown in table III-1, the range of variables included three levels of wheel angular velocity, three levels of flow rate, two blade heights, and three blade-to-housing axial clearances. Data for both radially inward and radially outward flow were taken for each test condition using the test apparatus shown in figure III-1. Static pressures, temperatures, and pressure fluctuations created by the passing blades were recorded at various radial stations. Torque was also recorded during each test.

The presentation and discussion of the results of this experimental program are divided into three categories: (1) static pressure distributions, (2) required torques, and (3) blade-to-blade pressure fluctuations.

B. STATIC PRESSURE DISTRIBUTIONS

A review of the results of a literature survey showed that a reliable pressure prediction method requires an accurate description of the "apparent" vortex mode and fluid angular velocity for each of the test conditions. The term apparent is used to denote a simplified flow pattern that does not include recirculation within the flow passages. Methods used in attempts to measure recirculation flows actually disturb the flow streamlines and give some doubt as to the validity of the information.

The apparent vortex mode can be readily seen by plotting the test data on a curve of the difference in inlet head and the head at any given radial station versus the square of the radius at the particular radial

Table III-1. Summary of Test Data

Run No.	Nominal Axial Clearance, in.	Blade Height, in.	Shaft Speed, rpm	Flow Rate, gpm	Nominal Flow Coefficient	Reynolds No. x 10^6	Torque Coefficient
1.01	0.125	0	5425	15.4	0.0045	12.9	0.0031
1.02	0.125	0	5250	2.3	0.00072	18.3	0.00286
1.03	0.125	0	5250	0	0	16.9	0.00286
1.04	0.125	0	5600	17.2	0.0050	13.3	0.0030
1.05	0.125	0	6575	19.5	0.0049	16.3	0.0027
1.06	0.125	0	5525	17.6	0.0052	13.1	0.0032
1.07	0.125	0	6150	19.1	0.0052	12.8	0.0030
1.08	0.125	0	6500	20.0	0.0050	16.0	0.0029
1.09	0.125	0	7150	20.9	0.0048	18.2	0.0028
2.01	0.084	0	4900	15.4	0.0076	10.4	----*
2.02	0.084	0	4850	27.4	0.014	9.67	----
2.03	0.084	0	5250	14.7	0.0064	11.8	----
2.04	0.084	0	6100	27.7	0.011	13.2	----
2.05	0.084	0	6250	10.0	0.0035	16.97	----
2.06	0.084	0	6350	0	0	13.5	----
2.07	0.084	0	5650	0	0	20.7	----
3.01	0.040	0	3990	26.9	0.035	6.87	----
3.02	0.040	0	3975	14.6	0.0185	22.5	----
3.03	0.040	0	4025	3.0	0.0038	8.51	----
3.04	0.040	0	5190	20.0	0.0194	9.69	----
3.05	0.040	0	5225	11.8	0.0114	10.4	----
3.06	0.040	0	5225	3.0	0.0029	13.2	----
3.07	0.040	0	6150	17.3	0.0142	12.3	----
3.08	0.040	0	6250	9.7	0.0078	14.1	----
3.09	0.040	0	6300	3.0	0.0024	19.99	----
3.10	0.040	0	5200	0	0	16.4	----

* Dashed line denotes no torque reading at these test data points

Table III-1. Summary of Test Data (Continued)

Run No.	Nominal Axial Clearance, in.	Blade Height, in.	Shaft Speed, rpm	Flow Rate, gpm	Nominal Flow Coefficient	Reynolds No. x 10^6	Torque Coefficient
4.01	0.1245	0.1250	2940	43.5	0.0122	5.59	----
4.02	0.1245	0.1250	3270	20.2	0.0051	7.19	----
4.03	0.1245	0.1250	3000	3.2	0.009	10.5	----
4.04	0.1245	0.1250	4100	40.7	0.0082	8.94	----
4.05	0.1245	0.1250	4010	25.2	0.0052	9.84	----
4.06	0.1245	0.1250	4240	3.0	0.0058	20.0	----
4.07	0.1245	0.1250	4750	41.1	0.0071	11.5	----
4.08	0.1245	0.1250	4840	21.0	0.00357	15.0	----
4.09	0.1245	0.1250	5120	3.9	0.0062	24.3	----
5.01	0.063	0.1250	2000	44.3	0.0243	4.21	0.018
5.02	0.063	0.1250	2000	17.9	0.0098	4.33	0.019
5.03	0.063	0.1250	1975	0	0	5.28	0.019
5.04	0.063	0.1250	2900	43.9	0.0166	6.30	0.019
5.05	0.063	0.1250	2950	23.5	0.0876	6.73	0.019
5.06	0.063	0.1250	2825	0	0	8.71	0.019
5.07	0.063	0.1250	3850	38.0	0.0109	9.01	0.0201
5.08	0.063	0.1250	3900	21.0	0.0059	9.88	0.0194
5.09	0.063	0.1250	3850	0	0	15.4	0.0196
6.01	0.02	0.1250	2475	41.4	0.024	4.12	0.0152
6.02	0.02	0.1250	2575	20.9	0.0116	4.4	0.0140
6.03	0.02	0.1250	2575	2.2	0.0012	6.3	0.0150
6.04	0.02	0.1250	3700	42.4	0.016	6.4	----
6.05	0.02	0.1250	3425	22.2	0.0093	6.3	----
6.06	0.02	0.1250	3425	3.2	0.0013	9.4	----
6.07	0.02	0.1250	4525	42.7	0.013	8.4	----
6.08	0.02	0.1250	4525	21.9	0.0069	10.1	----
6.09	0.02	0.1250	4625	5.0	0.0015	18.4	----

* Dashed line denotes no torque reading at these test data points

Table III-1. Summary of Test Data (Continued)

Run No.	Nominal Axial Clearance, in.	Blade Height, in.	Shaft Speed, rpm	Flow Rate, gpm	Nominal Flow Coefficient	Reynolds No. x 10^6	Torque Coefficient
7.01	0.122	0.2500	2680	43.2	0.0089	5.3	0.034
7.02	0.122	0.2500	2570	21.2	0.0046	5.5	0.034
7.03	0.122	0.2500	2590	2.8	0.0006	7.7	0.033
7.04	0.122	0.25	3040	40.5	0.0074	6.5	0.035
7.05	0.122	0.25	3040	19.9	0.0036	7.3	0.035
7.06	0.122	0.25	3080	2.1	0.0004	11.9	0.035
7.07	0.122	0.25	3515	41.3	0.0065	7.7	0.035
7.08	0.122	0.25	3515	20.0	0.0031	9.1	0.035
7.09	0.122	0.25	3540	2.2	0.0003	15.4	0.034
8.01	0.067	0.25	2010	39.5	0.0128	4.0	0.025
8.02	0.067	0.25	2030	20.2	0.0065	4.2	0.025
8.03	0.067	0.25	2050	1.0	0.0003	4.8	0.026
8.04	0.067	0.25	2850	39.4	0.009	5.9	0.024
8.05	0.067	0.25	2850	19.9	0.0046	6.3	0.025
8.06	0.067	0.25	2900	0.9	0.0002	9.6	0.025
8.07	0.067	0.25	3655	39.2	0.0070	8.2	0.025
8.08	0.067	0.25	3640	19.8	0.0036	9.16	0.025
8.09	0.067	0.25	3620	2.2	0.0004	15.6	0.026
8.10	0.067	0.25	4135	51.8	0.0082	9.3	0.026
8.11	0.067	0.25	4045	25.4	0.0041	10.5	0.026
8.12	0.067	0.25	4010	2.5	0.0004	15.2	0.026

Table III-1. Summary of Test Data (Continued)

Run No.	Nominal Axial Clearance, in.	Blade Height, in.	Shaft Speed, rpm	Flow Rate, gpm	Nominal Flow Coefficient	Reynolds No. x 10^6	Torque Coefficient
9.01	0.024	0.25	2020	38.4	0.014	3.8	0.021
9.02	0.024	0.25	2050	20.5	0.0076	3.98	0.021
9.03	0.024	0.25	2030	2.0	0.00074	4.45	0.022
9.04	0.024	0.25	2830	39.0	0.0105	5.53	0.020
9.05	0.024	0.25	2860	19.5	0.0052	5.93	0.021
9.06	0.024	0.25	2860	1.6	0.0004	7.73	0.021
9.07	0.024	0.25	3590	38.8	0.0082	7.45	0.020
9.08	0.024	0.25	3630	20.0	0.0042	8.37	0.021
9.09	0.024	0.25	3660	1.9	0.00039	12.8	0.020
10.01**	0.067	0.125	2040	37.5	0.0195	3.92	0.021
10.02	0.067	0.125	2050	20.3	0.0105	4.30	0.021
10.03	0.067	0.125	2035	2.1	0.00109	4.67	0.021
10.04	0.067	0.125	2815	41.4	0.0156	5.57	0.021
10.05	0.067	0.125	2805	20.2	0.007	5.90	0.021
10.06	0.067	0.125	2820	2.2	0.00082	7.76	0.021
10.07	0.067	0.125	3590	39.7	0.0118	7.55	0.020
10.08	0.067	0.125	3625	20.0	0.0059	8.58	0.021
10.09	0.067	0.125	3670	1.6	0.00046	15.1	0.021
10.10	0.067	0.125	4540	39.8	0.0093	10.6	0.020
10.11	0.067	0.125	4505	19.8	0.0047	12.7	0.021
10.12	0.067	0.125	4670	1.5	0.0003	27.9	0.019

** - 12 blades

Table III-1. Summary of Test Data (Continued)

Run No.	Nominal Axial Clearance, in.	Blade Height, in.	Shaft Speed, rpm	Flow Rate, gpm	Nominal Flow Coefficient	Reynolds No. x 10^6	Torque Coefficient
11.01***	0.067	0.125	2060	32.4	0.0166	4.27	0.018
11.02	0.067	0.125	2070	19.5	0.0099	4.36	0.018
11.03	0.067	0.125	2060	2.1	0.00107	4.86	0.019
11.04	0.067	0.125	2840	42.5	0.0158	5.99	0.018
11.05	0.067	0.125	2850	20.2	0.00749	6.31	0.018
11.06	0.067	0.125	2840	1.6	0.00059	7.62	0.018
11.07	0.067	0.125	3650	40.2	0.0116	8.07	0.017
11.08	0.067	0.125	3640	20.5	0.0059	8.80	0.017
11.09	0.067	0.125	3630	4.0	0.00116	11.3	0.017
11.10	0.067	0.125	3860	3.9	0.00106	12.2	0.015
11.11	0.067	0.125	5095	41.1	0.00853	12.8	0.015

*** - 6 blades

station. In subsequent discussion, this type of plot will be referred to as ΔH-R^2 curves. A straightline distribution on this curve indicates a forced vortex. A curved line indicates the existence of some other vortex mode such as free, superforced, or various levels between these extremes.

The experimental program was conducted only with water at ambient temperatures. Therefore, all results and conclusions reported herein apply only to uncompressible fluids. This work should be extended to include compressible fluids such as liquid hydrogen.

For purposes of analysis, the test results are shown in terms of impeller head distributions where head is in feet of water. For the range of test conditions considered in this water program, the density of the fluid remained constant and, therefore, permits the following simple conversion

$$H/P = 144/\gamma = 2.32.$$

1. Smooth Impeller Tests

The first phase of the experimental program was initiated with tests of the smooth disk at various disk-to-housing axial clearances. All smooth disk data for radially outflowing fluid resulted in straightline ΔH-R^2 plots except in the area just downstream of the eye of the impeller. A typical ΔH-R^2 plot is shown in figure III-2. Therefore, it can be concluded that a forced vortex existed over most of the disk's radial span, and the fluid reached its maximum angular velocity soon after entering the impeller. The momentum losses at the inlet result from the rapid turn of the fluid from an axial to a radial direction; this will be investigated more thoroughly in a later program.

Once it is established that the flow is a forced vortex, it is a straightforward matter to calculate the average fluid velocity between the disk and housing. The fluid "core rotation" or fluid angular velocity is:

$$\beta = [2\ g(H_2 - H_1)/(R_2^2 - R_1^2)]^{1/2}.$$

For convenience, a nondimensional fluid velocity, K, is defined as the fluid angular velocity divided by the wheel or impeller angular velocity or,

$$K = \beta/\omega.$$

As stated before, it was found that for the smooth disk and radial outflow, K remained constant with respect to radial span; however, the disk-to-housing clearance and flow coefficient had a measurable effect. Since at any particular radius,

$$\beta = C_u/R,$$

and

$$\omega = u/R;$$

then

$$K = C_u/u.$$

Using the data from the smooth disk tests, a graph was constructed to show the effects of flow coefficient (Cm/u) defined at the impeller tip, on K for various clearances. These curves are shown in figure III-3. They can be extrapolated and interpolated to provide the more convenient graph of figure III-4, which shows even increments of axial disk-to-housing clearances.

The only data that can be compared with these experimental results comes from a study conducted by Daily and Nece (Reference 2). These investigators did not permit any through flow in their tests, so data

collected on the current program can only be compared at shutoff flow ($Q = 0$). The effect of axial disk-to-housing clearance and disk radius on fluid velocity ratio is shown in figure III-5, along with the theoretical and experimental data of Daily and Nece. Since the values of C_A/R used in this experiment were restricted to typical centrifugal pump backface applications, the data are not extensive enough to make a complete comparison. The test curve from this experiment, as shown in figure III-5, tends to fall lower and slope downward more severely as compared to the data of Daily and Nece. But, in general, for the range of C_A/R tested in this program, the correlation is considered quite good. This correlation is shown only for academic reasons, since rocket engine pump impellers (front or back faces) seldom operate at shutoff flow.

In the analysis of the data produced by the smooth disk for radially inflowing fluid, the ΔH-R^2 plots for each of the tests revealed a changing curvature as flow coefficient was altered. Close examination showed that in each case, the curve was straight at shutoff flow, but became a curved line as flow coefficient was increased. (See typical curve in figure III-6.) Therefore, it was obvious that the vortex mode for radially inflowing fluid was changing with flow coefficient and was progressing from a forced vortex at shutoff flow toward a free vortex as flow rate was increased.

In vortex flow

$$Cu\ R^n = \text{Constant},$$

and

$$\int dP/\gamma = \frac{1}{2g} \int \beta^2\ RdR.$$

These equations can be solved in terms of "n" if the radial static pressure distribution and the fluid velocity at a particular radius, are

known. The fluid velocity in these tests was obtained from a tangential total pressure probe at the tip of the impeller. The static pressure measurements were obtained from the static taps, which were discussed in the section describing the test apparatus. Using the data produced by this experimental program and the preceding two theoretical relationships for vortex motion, a curve was developed showing the effect of flow coefficient on the vortex exponent, "n," for various clearances. This curve is shown in figure III-7. The effect of flow coefficient and axial disk-to-housing clearance on fluid velocity ratio, K, is given in figure III-8. The data from the intermediate clearance test had to be discarded because of the loss of the total pressure tap at the impeller tip and the data shown on figures III-7 and III-8 are not complete. In addition, a wide range of flow coefficients for the high axial clearance was not possible because of flow limitations of the facility pump. It was noted that the value of Cu_o did not approach 0.50 for the inward flow, as did the Cu_o from the outward flow data at the shutoff flow condition. An instrument error is suspected; however, it was noted in the literature that a similar discrepancy was reported by Maroti, et al, (Reference 7). Maroti reasoned that the end effects associated with the partially enclosed disk as compared with the fully enclosed disk would cause the discrepancy.

As stated before, the ΔH - R^2 curves at zero flow were straight lines, a phenomenon that is indicative of an existing forced vortex motion. Knowing that a forced vortex mode existed for that particular

test point, the fluid velocity that must exist at the impeller tip can be calculated from the static pressure drop. This value can then be compared to the fluid velocity indicated by the total and static pressure probes for that particular test point. The ratio of these two calculated values of fluid velocity is an indication of the probe angular orientation with the actual flow direction, and therefore, an indication of the probe accuracy for that particular rig assembly. (This fact was verified with bench tests of the same rig probe under controlled conditions over the range of velocities encountered in this test program.) This ratio, or correction factor, was then applied to all ensuing measured fluid velocities at the impeller tip to determine the true value.

2. Bladed Impeller Tests

A series of tests was conducted at three impeller speeds, three flow rates and using three different blade tip-to-housing clearances. The resulting data were treated in a manner similar to that employed with the smooth impellers; i.e., $\Delta H - R^2$ curves were plotted and values of K were calculated for the various test conditions. Typical examples of these plots are shown in figures III-9 and III-10. The fact that these data lie along a curved line show that the fluid angular velocity does not remain constant over the radial span of the impeller as was expected. (The $\Delta H - R^2$ curve is straight only if the fluid angular velocity is constant.) It was noted from the data that the three variations of the flow rate for each of the test speeds produced no significant variation in the $\Delta H - R^2$ curves; therefore, the fluid velocity ratio, K, was considered to be

independent of flow coefficient in the range of $\phi = 0$ to $\phi = 0.02$ for bladed impeller configurations. The ratio of blade height to blade height plus tip clearance, T/S, was found to have an appreciable effect on values of K; for increasing values of T/S the associated value of K at a particular radius would also increase.

The test results for this series of bladed impeller tests are shown in figures III-11 and III-12. It should be pointed out that these curves represent the best statistical curve fit for all data produced in this series of tests. Each $\Delta H - R^2$ curve was generated by four pressure measurements. Then, each curve was read at increments of 2 in.^{2} and fluid velocity ratios were calculated. For one clearance case, or one T/S, nine $\Delta H - R^2$ plots were generated providing up to 90 individual values of K for each T/S. These data were then input into an IBM statistical curve fit using a second order polynomial equation form. The resulting equations are plotted in figures III-11 and III-12. The maximum deviation between actual test data and these curves is 3%.

Comparing the results of figures III-11 with III-12, it was found that there is no difference in fluid velocity ratio between inward and outward flow within the accuracy of the test data. A composite curve was, therefore, produced, which applies to both radially inward and radially outward flow. This curve is shown in figure III-13.

Some concern quite naturally resulted when the variation in fluid velocity with radial span was encountered. To make sure this effect was not caused by a momentum transfer between the fluid in the annular

area above the impeller and the fluid just leaving the impeller, another plot of fluid velocity ratio, K versus T/S for various radius ratios, was produced as shown in figures III-14 and III-15. If the indicated slopes of the curves are extended, each curve passes through K = 1 at T/S = 1. This is as it should be and indicates the fluid velocities in this test were controlled by T/S alone and were not influenced by recirculation flows or momentum transfer at the impeller tip.

Tests with the next impeller configuration followed using a bladed disk with 24 0.250-inch blades. Again, three tests were conducted with three different axial blade tip-to-housing clearances. Data were produced at three flow rates and three speeds in each test. The same method of data analysis was used as in the previous 0.625-inch blade tests. However, the results were quite different in that there was no uniform trend of fluid velocity ratio, K, for various T/S cases. The effect of radial span on fluid velocity ratio was again encountered, but the fluid velocities seemed to be independent and not consistent with varying T/S values. The statistical curves developed from the test data are shown in figures III-16 and III-17. Note that the curves for T/S = 0.67 did not return to K = 1 at low radius ratios. A speed measurement error was suspected in this test but could not be definitely proved. It is believed that these curves should be shifted upward so that K = 1 at low radius ratios.

Once the preceding adjustment had been made, there appeared to be no significant difference in the various curves for different T/S values. The data for all T/S values was collected and input into the statistical curve fit program. The resulting equation is plotted in figure III-18 and applies to both radially inward and radially outward flow directions.

The final phase of the experimental program comprised a study to determine the effect on the radial pressure distribution of changing the number of blades. The 24-blade impeller with 0.125-inch blade heights was used for this portion of the experimental investigation. Blade tip-to-housing axial clearance of 0.067 inch was used for all tests in this series. Every other blade on this impeller was removed, leaving 12 equally spaced blades. This configuration was tested at three speeds and three flow rates. For the final test, six additional blades were machined from the impeller and the new configuration was tested at three speeds and three flow rates. The results of these tests are shown by figures III-19 and III-20. Notice that the curves for 12 and 6 blades did not return to K = 1 at low radius ratio. A speed error was again suspected, and the curves were shifted vertically to the point where the low radius ratio portion of the curves coincided with the line K = 1. The shifted curves are shown in figure III-21, and these curves show that the effect of reducing the number of blades is relatively small, provided $N \geq 6$. This observation is consistent with results reported by other investigators such as Stepanoff and Acosta.

C. TORQUE MEASUREMENTS

The torque data obtained from each test were plotted as torque coefficient, C_M, versus disk Reynolds number, Rey, at the tip for the smooth disk and the bladed disk. The smooth disk torque data are presented in figure III-22. Torque data for two of the three smooth disk tests were not available due to a failure of the torque recording device during these tests. Fair agreement was found by comparison with the data of Daily and Nece (Reference 2), and with the theoretically derived equation by Schultz-Grunow (Reference 5). Various axial clear-

ances did not have an appreciable effect on the frictional resistance, and there was also no noticable change with increasing flow rate for the low flow coefficients investigated (below 0.02). The bladed disk torque data were analyzed in the same manner as the smooth disk, and the results are presented in figure III-23. Similarly, the bladed data were not noticably affected by varying flow rate for the low flow coefficients investigated. A significant effect of T/S and blade height was apparent from the data. A curve for the roughened disk torque reported by Daily and Nece is also shown on figure III-23.

The torque measurements included the edge drag of the disk, so a calculation of disk edge friction was necessary for a valid comparison of data. The method of Daily and Nece (Reference 2) for turbulent flow was used in this calculation. The method considers the annulus between the disk and the wall as a duct analogous to a circular pipe. The shear stress on the disk tip was given as,

$$\tau = (f/4)\ (\rho/2)\ (\omega R_o/2)^2.$$

This expression is used in deriving the correction for C_M expressed as,

$$C_M' = \frac{f\ \pi\ b}{8\ R_o}$$

and, hence,

$$C_{M\ actual} = C_{M\ measured} - C_M' .$$

The friction factor, f, was determined from the smooth pipe curve on a Moody diagram using a Reynold number given as,

$$Rey = \frac{\omega R_o\ C}{\nu}$$

Daily and Nece found by experimenting with smooth disks of various thickness that this correction method was valid. Values of C_M' for the testing performed in this report ranged from 0.0010 to 0.00133.

The data from figure III-23 are plotted in another form in figure III-24, which shows torque coefficient versus T/S. Notice the decrease in C_M as T/S is increased, as would be expected. Also notice that the moment coefficient at any given T/S is higher for 0.250-inch blade height than for 0.125-inch blade heights. This result is thought to be an indication of the fluid recirculation that predominates in the case of the wider blade passage. This conclusion is consistent with the results seen earlier when the fluid velocities for the 0.250-inch blade heights were inconsistent as compared to the 0.125-inch blade height tests.

D. BLADE-TO-BLADE PRESSURE FLUCTUATIONS

High response transducer data were obtained with Kistler Model 601A quartz pressure transducers close coupled with the Model 624 adapter. The transducers were located on four radii on the front housing and mounted flush with the wall surface. The output of the transducers was recorded on frequency-modulated tape, which was later analyzed by an oscillograph and a panoramic wave analyzer. The oscillograph recording was obtained using a 100 cps high pass filter in an attempt to separate the pressure wave caused by the blade from a low frequency relatively high amplitude pressure oscillation, which was noticed on all of the bladed test runs. The oscillograph recording showed the true pressure pulse across the blade. However it was modulated by the low-frequency pulses and as a result the amplitude was not constant . Figures III-25 and III-26 show a portion of the oscillograph recording from typical tests. The panoramic wave analyzer was used to separate the various components of the pressure

pulse wave, and from them determine the amplitudes at the predominent frequencies. A typical plot obtained from the panoramic wave analyzer is shown in figures III-27 and III-28. The predominant frequencies were the blade passing frequency, ω_B, the higher harmonics and the low frequency between 40 and 50 cps.

For each of the bladed test runs, a pressure parameter was calculated using the peak-to-peak amplitude of the pressure pulse at the blade passing frequency divided by the static pressure at the particular radius. The results of this calculation are shown graphically in figure III-29 as $\Delta P/P$ versus radius ratio.

FD 5510

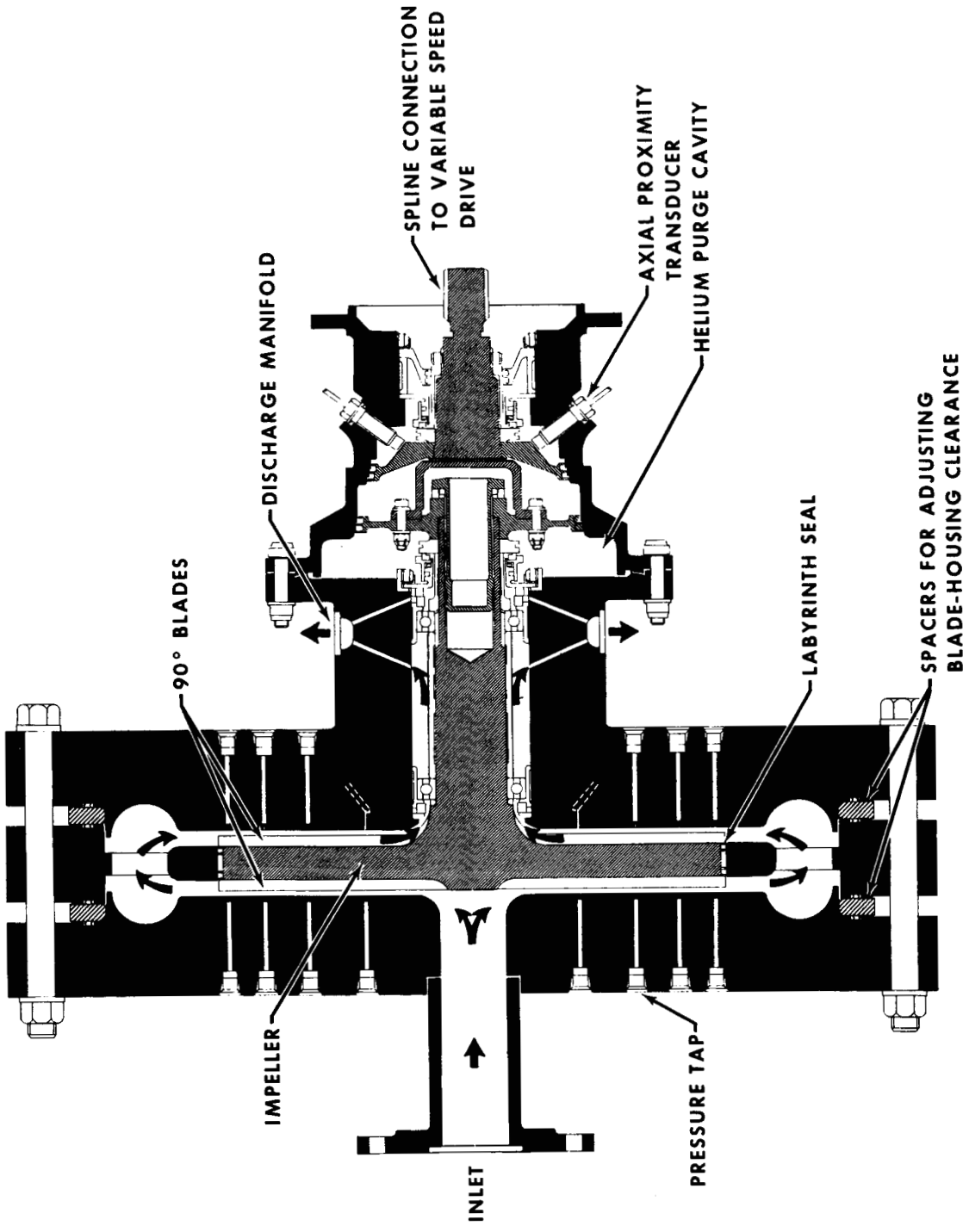

Figure III-1. Radial Pressure Distribution Rig Showing Direction of Flow

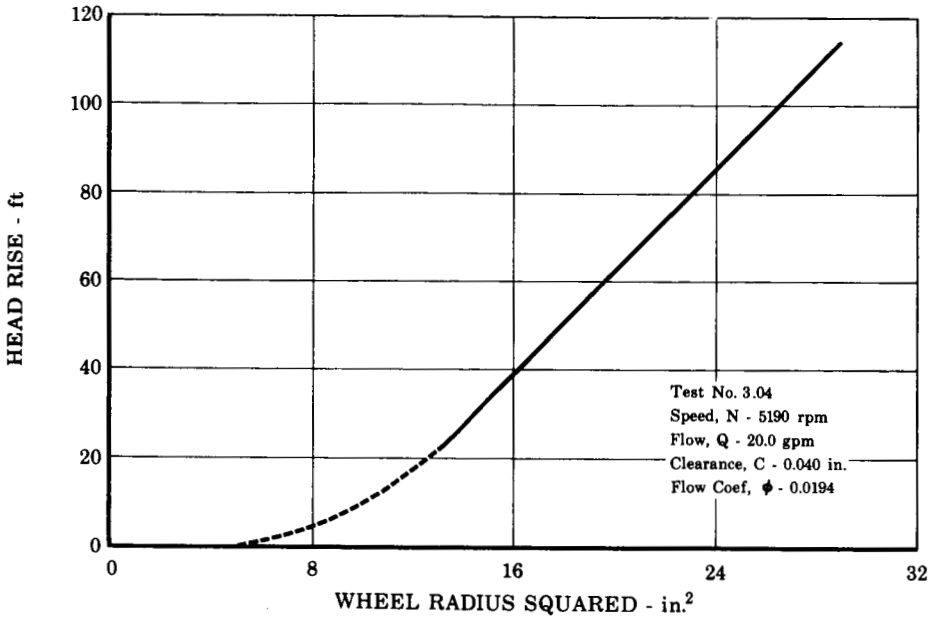

Figure III-2. Head Rise vs Wheel Radius Squared for Smooth Disk Rotor, Radially Outward Flow FD 7814

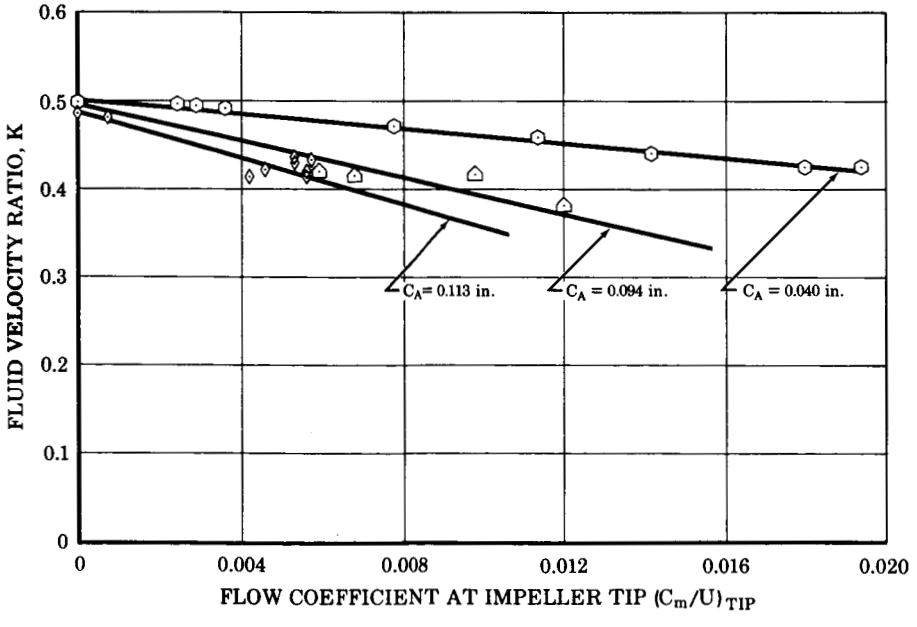

Figure III-3. Effect of Ratio of Fluid Tangential Velocity at Impeller Tip with Flow Coefficient at Tip FD 7815

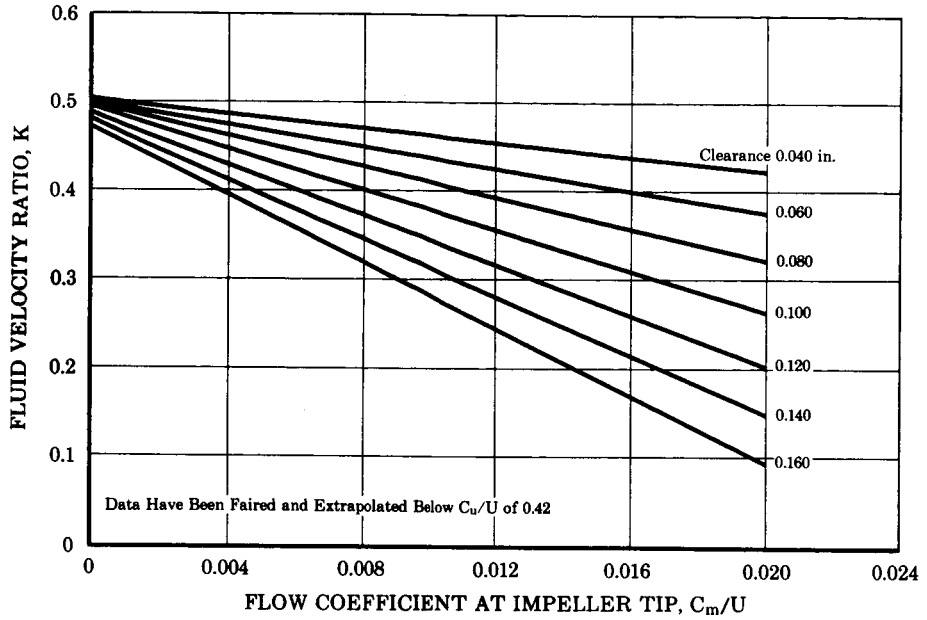

Figure III-4. C_u/U vs C_m/U for Radially Outward Flow on a Smooth Disk FD 7816

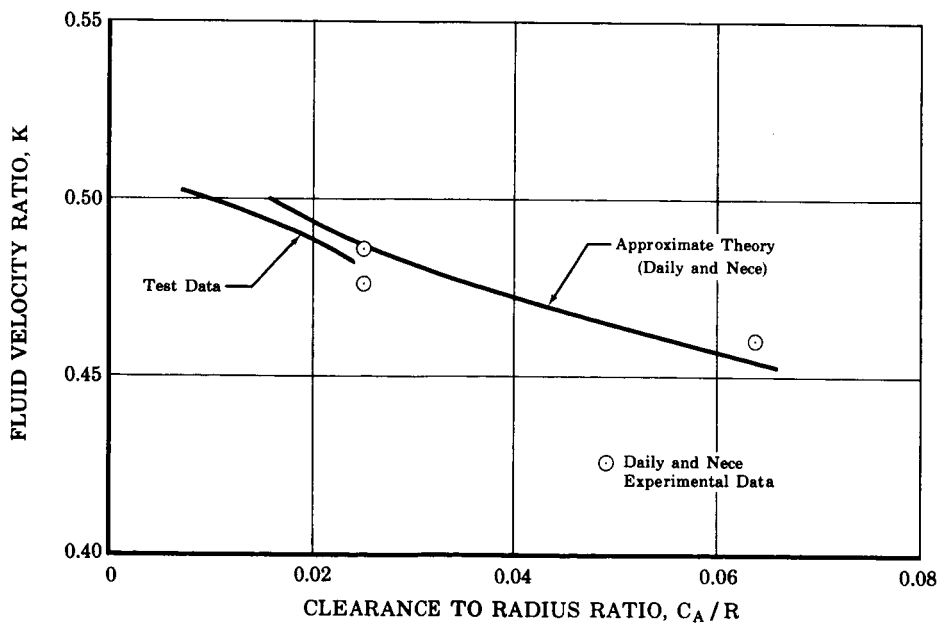

Figure III-5. Smooth Disk C_u/U at Shutoff Flow FD 7817

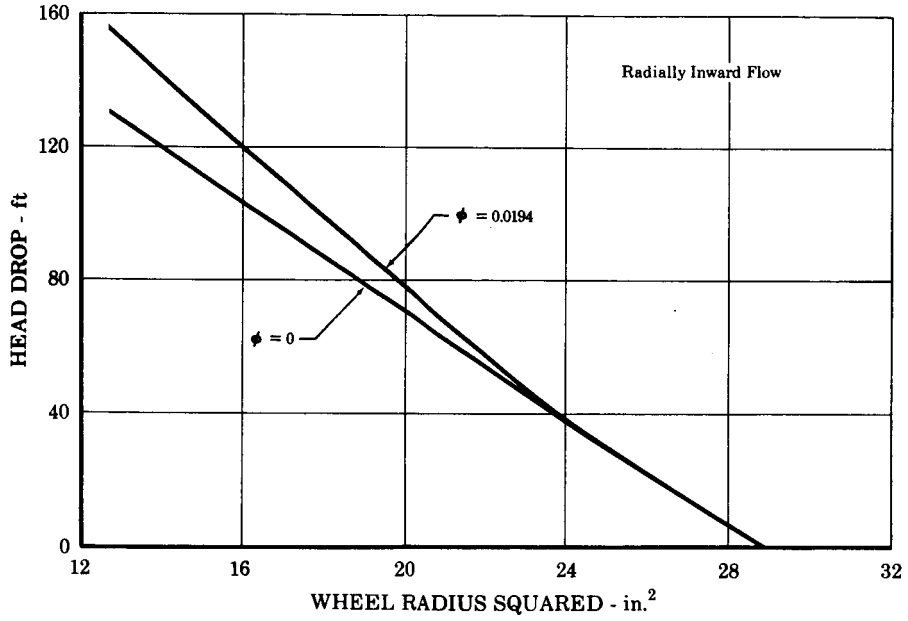

Figure III-6. Head Rise vs Wheel Radius Squared for Smooth Disk Rotor FD 7818

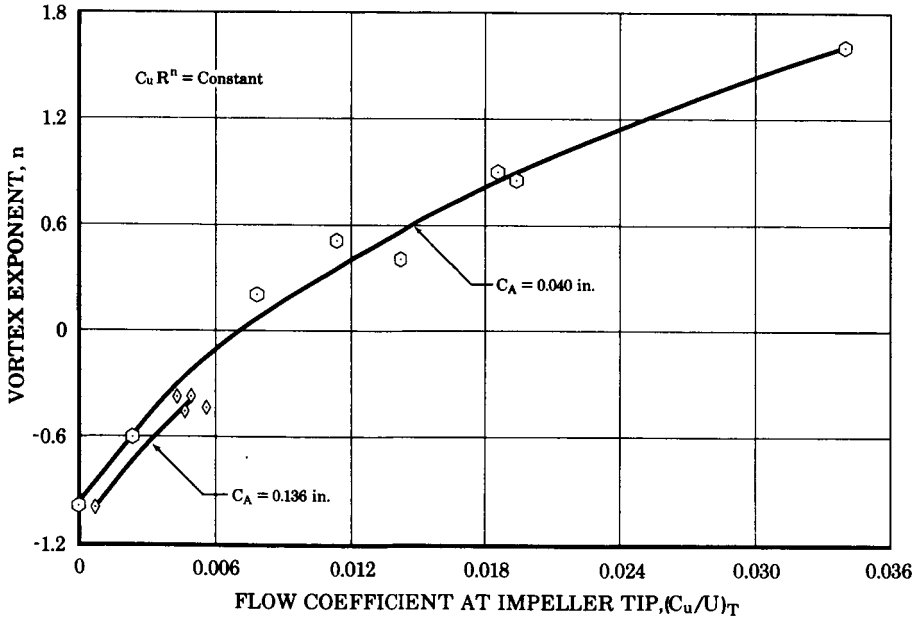

Figure III-7. Effect of Flow Coefficient at Impeller Tip on Vortex Mode FD 7819

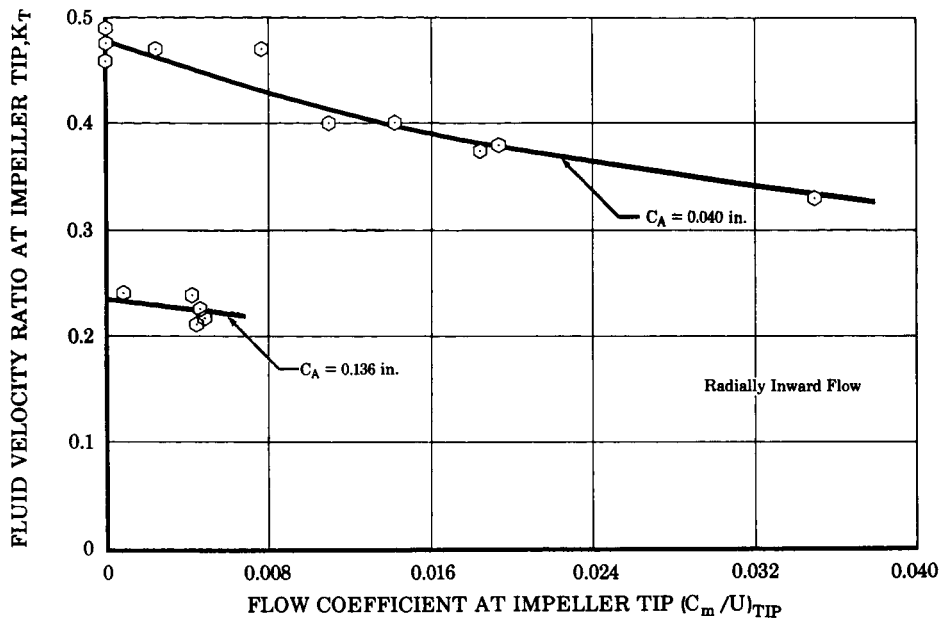

Figure III-8. Effect of Ratio of Fluid Tangential Velocity to Wheel Tangential Velocity at Impeller Tip with Flow Coefficient at Impeller Tip FD 7820

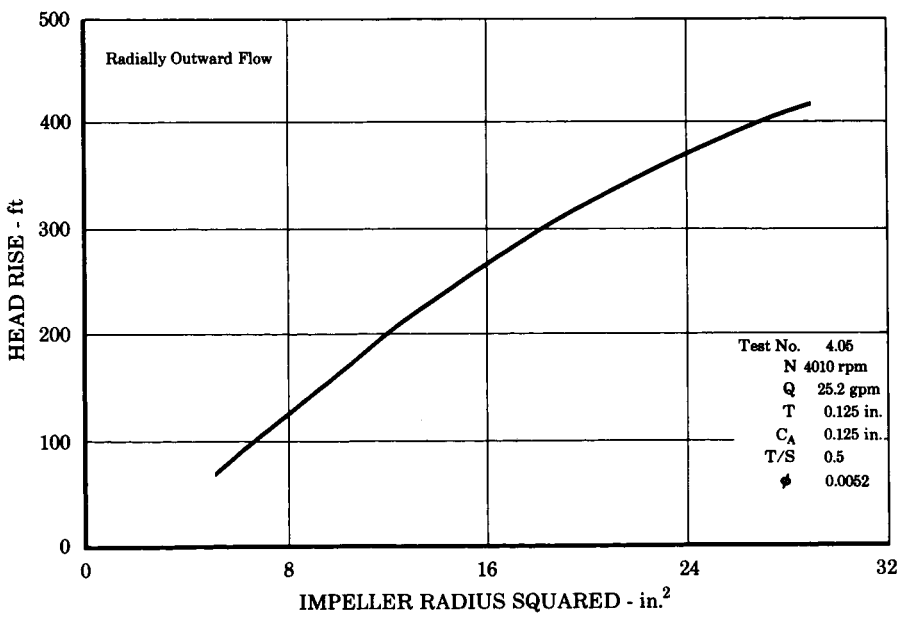

Figure III-9. Radial Pressure Distribution for Bladed Impeller FD 7840

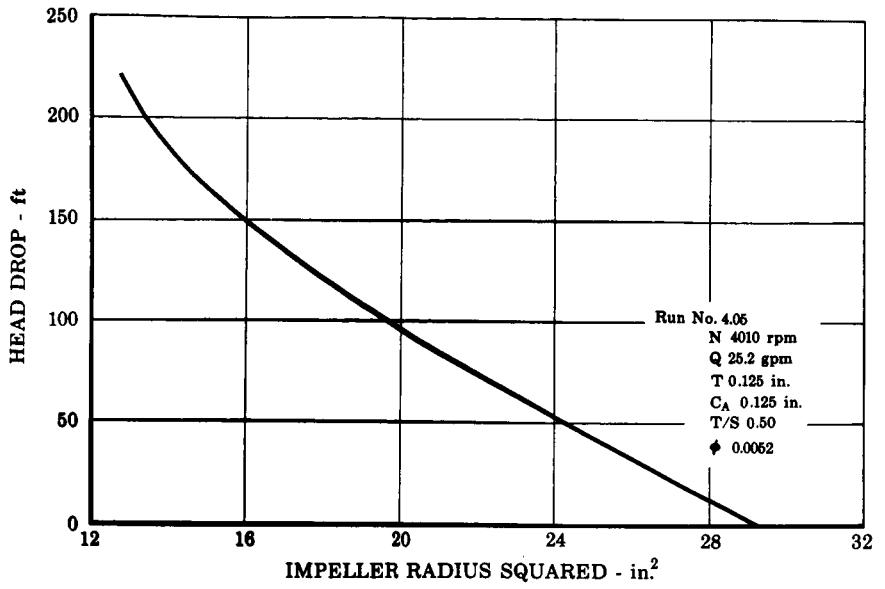

Figure III-10. Radial Pressure Distribution for Bladed Impeller, Radial Inward Flow FD 7821

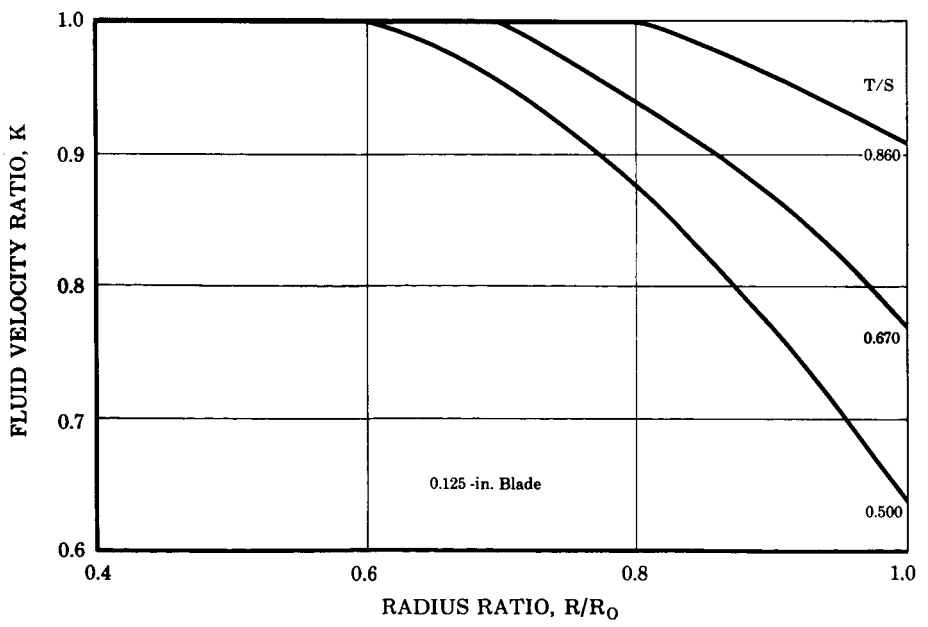

Figure III-11. Fluid Velocity Ratio vs Radius Ratio for Radially Outward Flow FD 7822

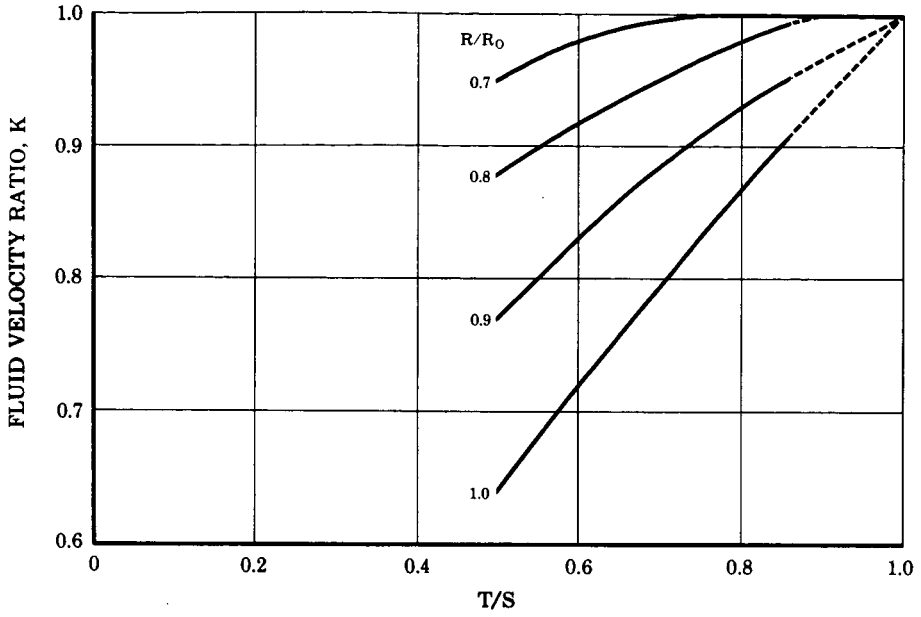

Figure III-14. Fluid Velocity Ratio vs T/S for Radially Outward Flow FD 7825

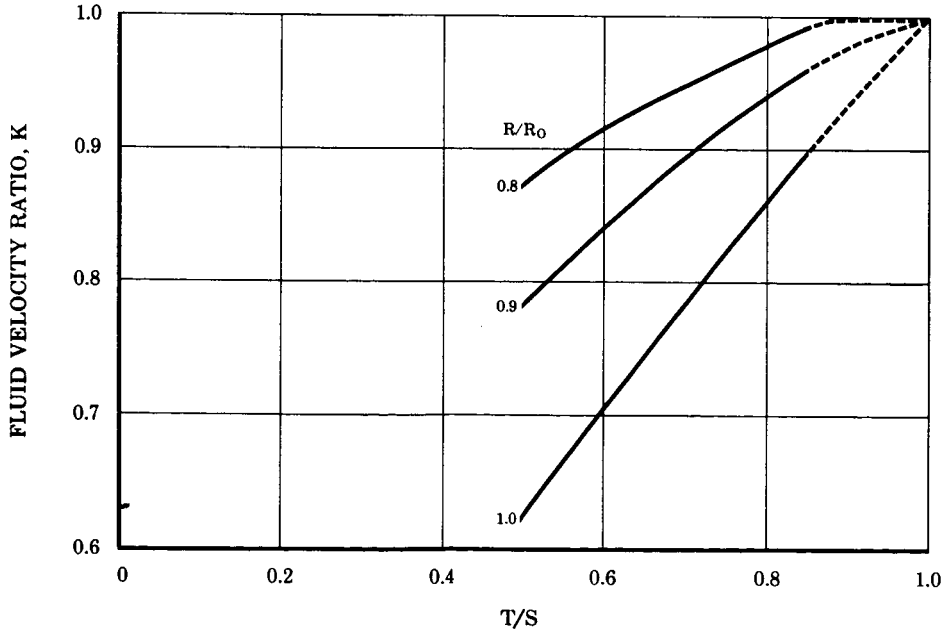

Figure III-15. Fluid Velocity Ratio vs T/S for Radially Inward Flow FD 7830

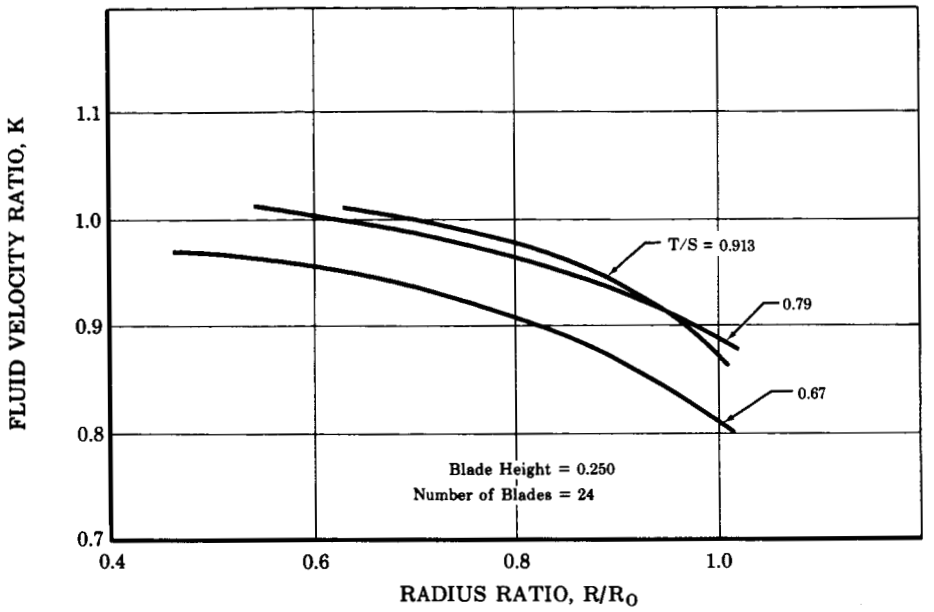

Figure III-16. Fluid Angular Velocity Correlation for 24-Blade, 0.250-in. Impeller (Outward Flow) FD 7831

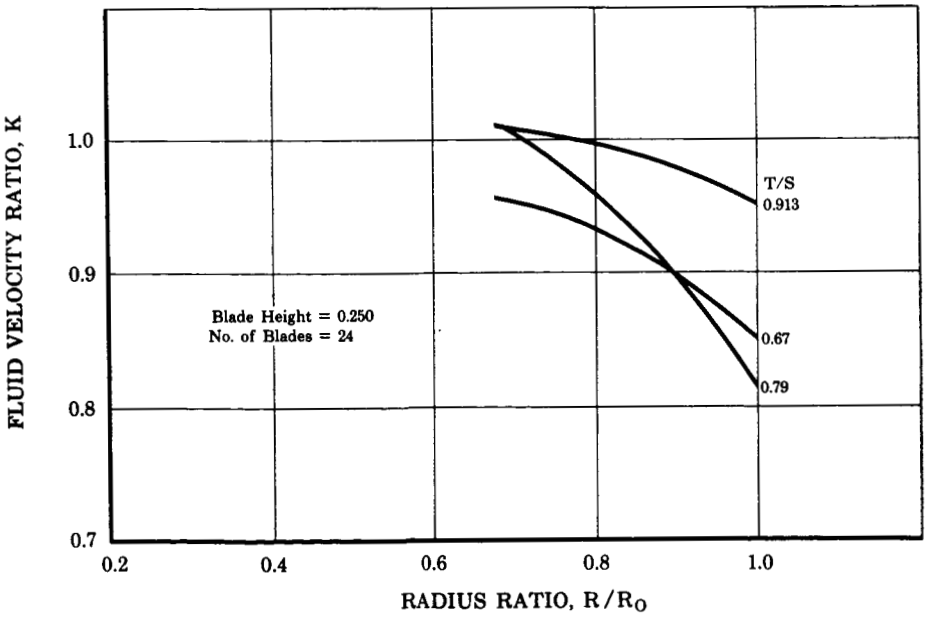

Figure III-17. Fluid Angular Velocity Correlation for 24-Blade, 0.250-in. Impeller (Inward Flow) FD 7832

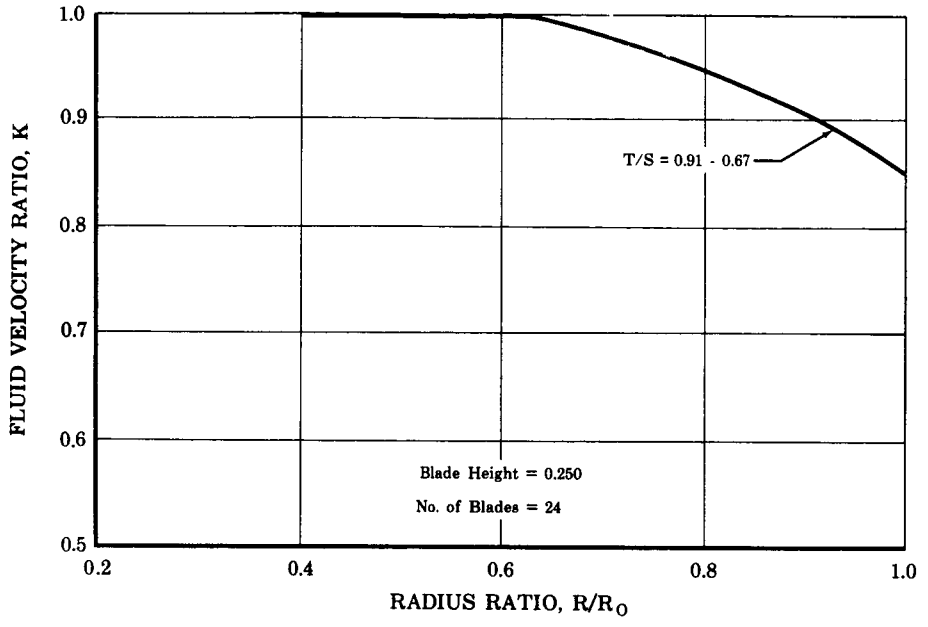

Figure III-18. Fluid Angular Velocity Correlation for 24-Blade, 0.250-in. Impeller (Inward or Outward Flow) FD 7833

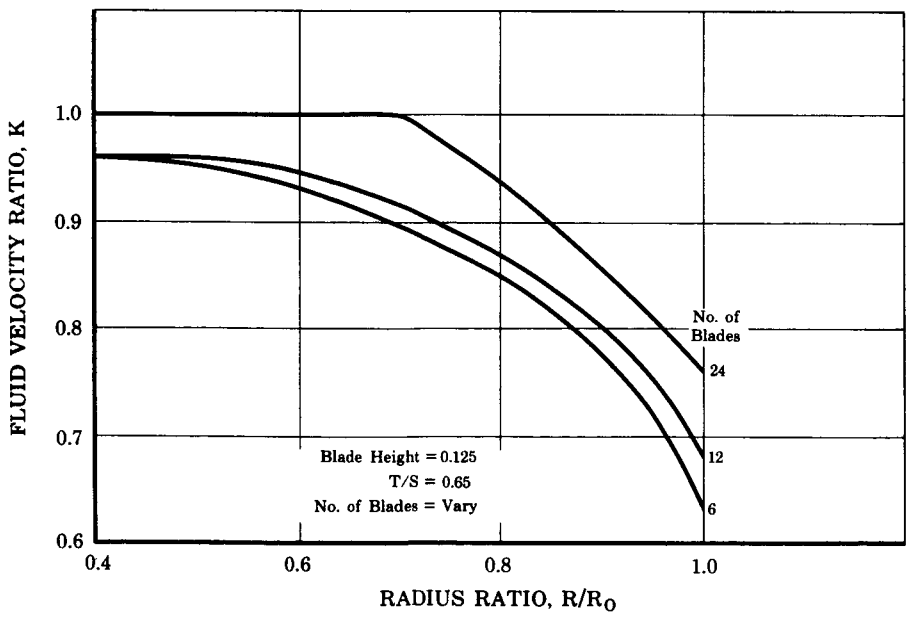

Figure III-19. Fluid Angular Velocity Correlation (Effect of No. Blades, Outward Flow) FD 7834

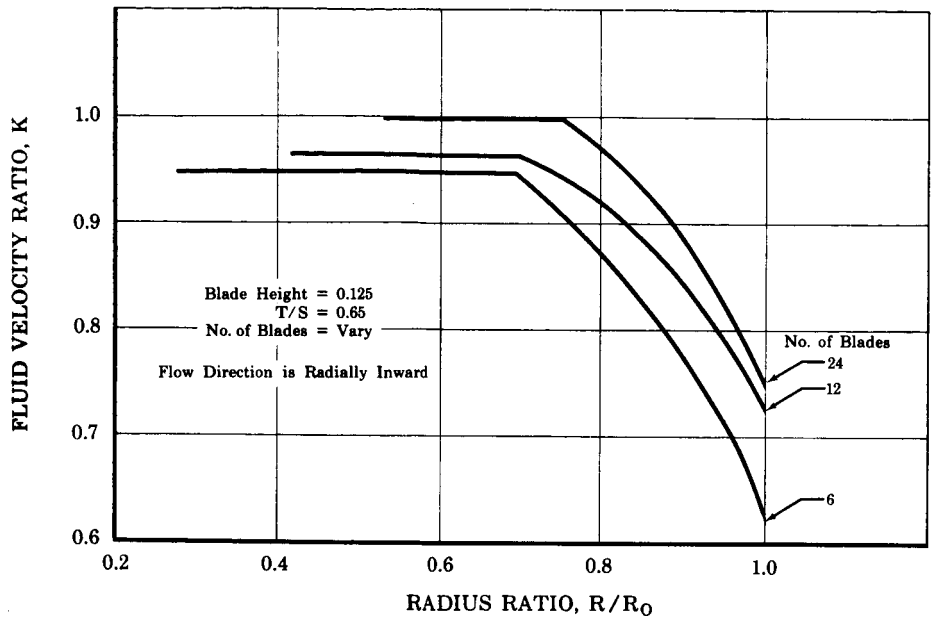

Figure III-20. Fluid Angular Velocity Correlation FD 7835
(Effect of No. Blades, Inward Flow)

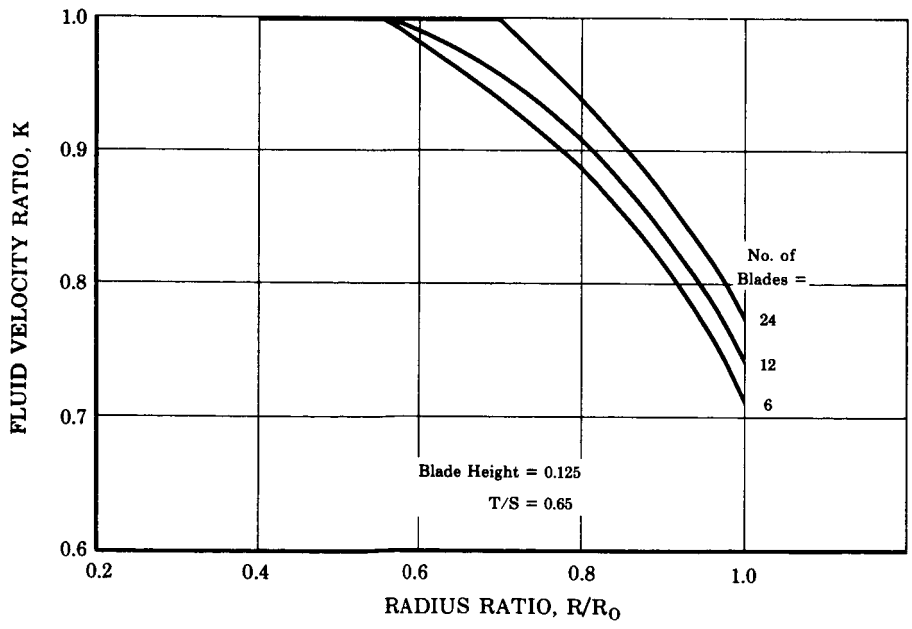

Figure III-21. Fluid Angular Velocity Correlation FD 7836
(Inward or Outward Flow, Various No.
of Blades)

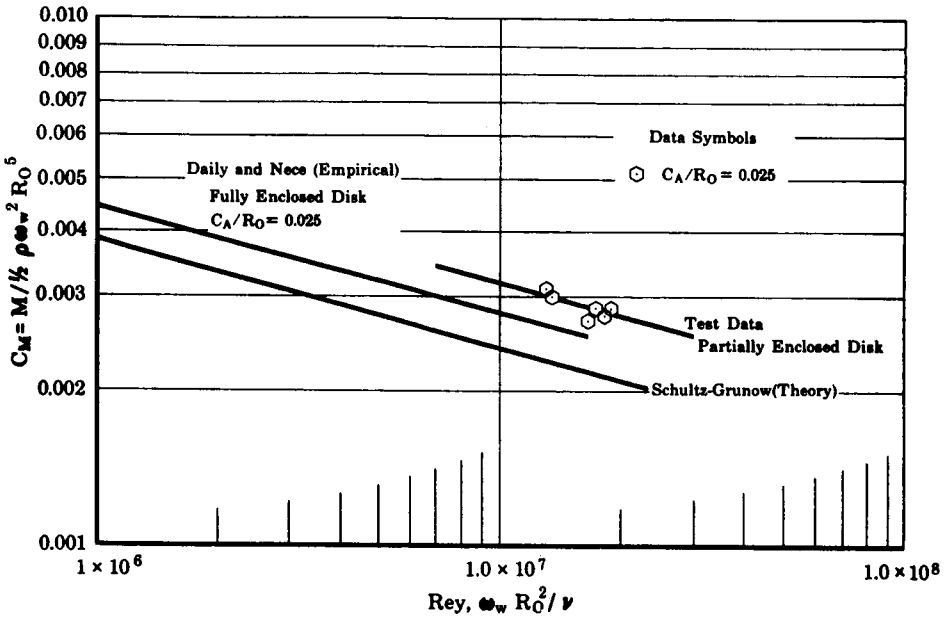

Figure III-22. Smooth Disk Torque Data FD 7837

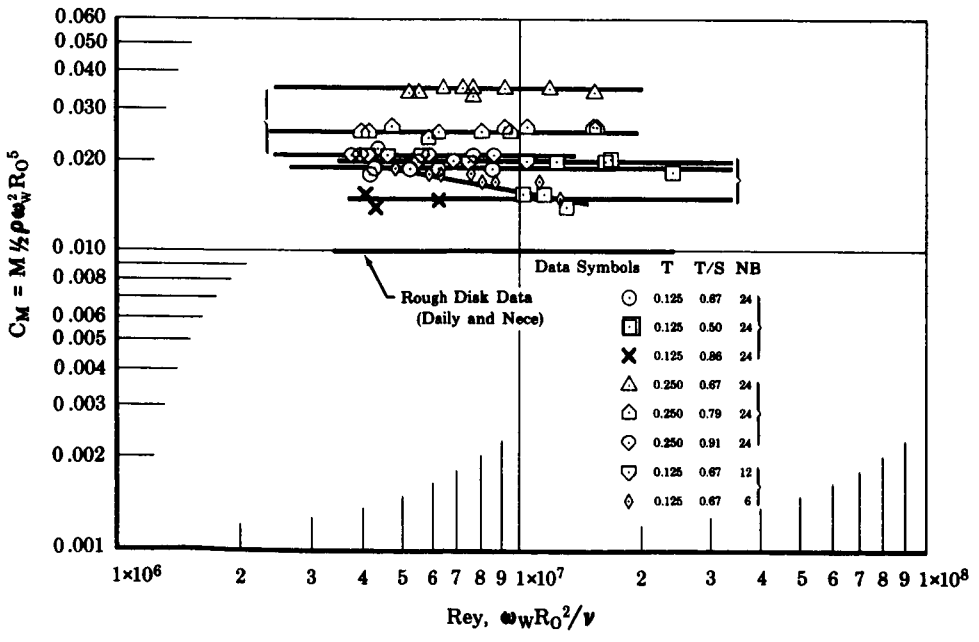

Figure III-23. Bladed Disk Torque Data FD 7838

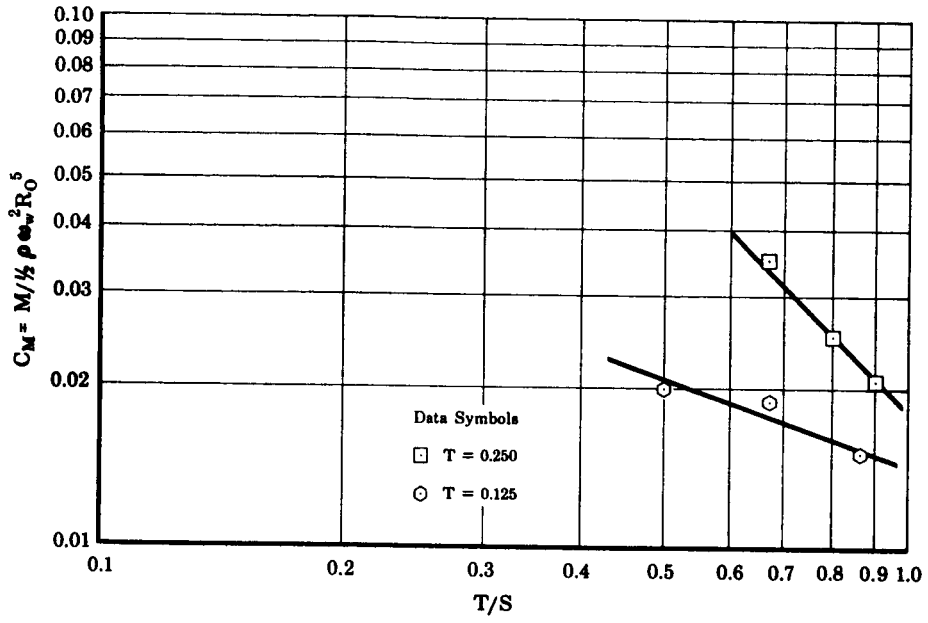

Figure III-24. Correlation of C_M with T/S for 24-Blade Impeller FD 7839

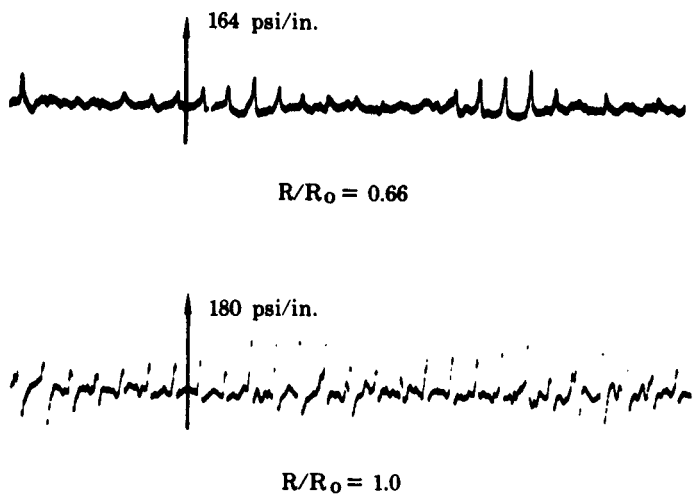

Figure III-25. Oscillograph Analysis of Test No. 11.09 ω_B = 363 cps FD 7826

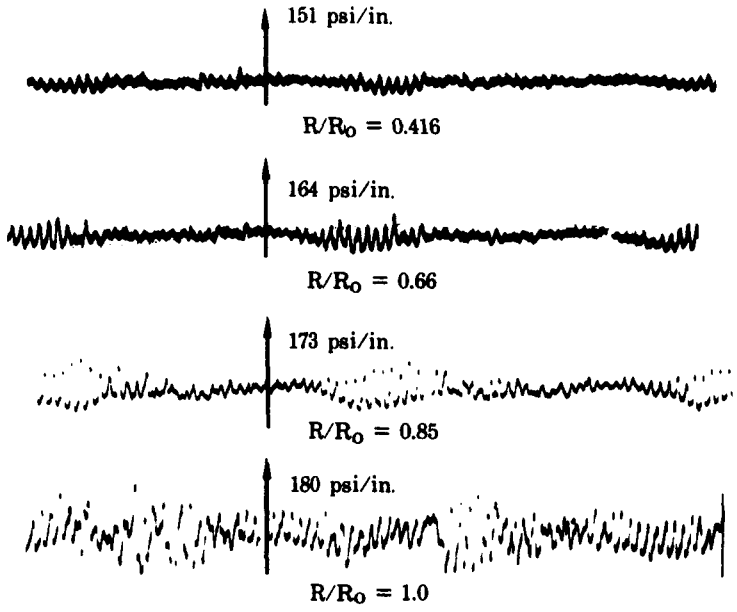

Figure III-26. Oscillograph Analysis of Test No. 4.08 ω_B = 1940 cps FD 7827

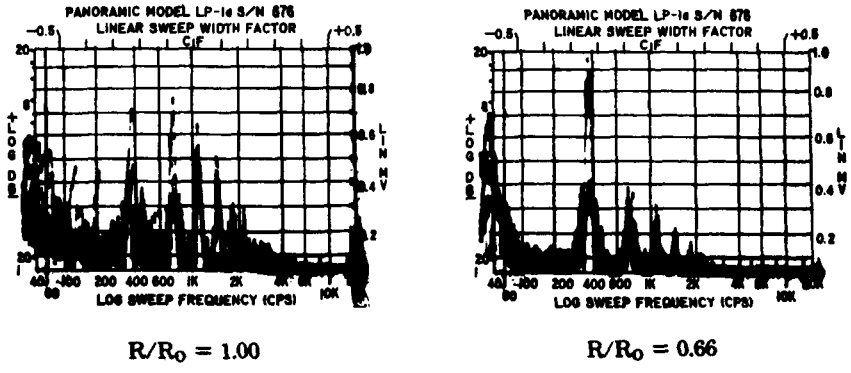

Figure III-27. Panoramic Wave Analysis of Test No. 11.09 ω_B = 363 cps Scale = 0-50 psi FD 7828

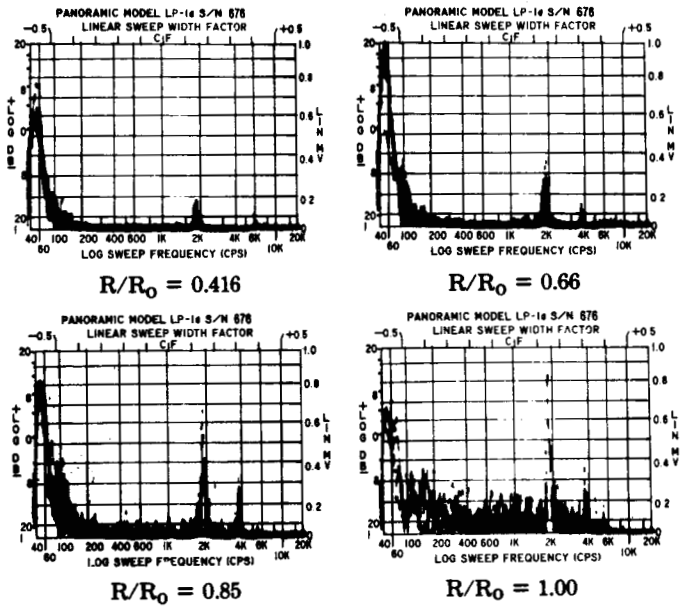

Figure III-28. Panoramic Wave Analysis of Test No. 4.08 FD 7829

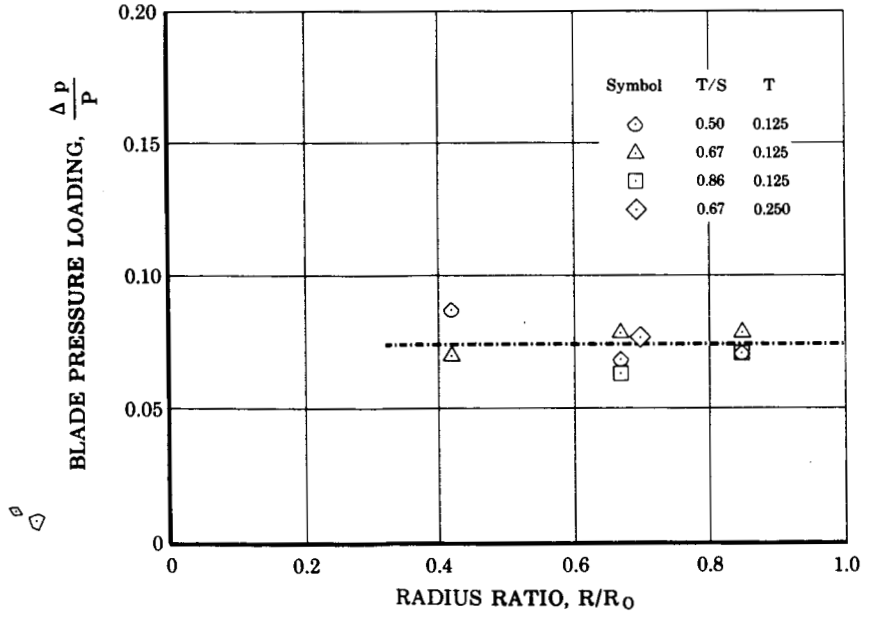

Figure III-29. Blade Pressure Loading FD 7812

SECTION IV
PRESSURE DISTRIBUTION PREDICTION METHODS

A. GENERAL

The following methods of predicting pressure distribution generated by low flow pumping surfaces have been formulated from the experimental results produced in this program. These methods apply to incompressible fluids only. They are empirical in nature and presented basically in graphical form. It should be noted that the methods discussed below are preliminary and are intended to serve as a basis for a more complete prediction system that would result from additional testing. This should include additional water tests to determine impeller end effects and liquid hydrogen tests to determine the effects of compressibility.

B. RADIALLY OUTFLOWING FLUID PASSING A ROTATING SMOOTH FACE

As discussed in Section III (Experimental Results), a forced vortex was found to exist for all cases tested and the prediction system was dependent on defining the magnitude of the fluid angular velocity between the disk and housing. This value can be found by referring to figure III-4, which shows the ratio of the fluid angular velocity to the impeller angular velocity, K, as a function of flow coefficient, C_m/u, and axial clearance, C_A. The fluid angular velocity, β, is then found by the following relationship:

$$\beta = K\omega$$

The distribution in head between R_2 and R_1 is then found by the forced vortex equation,

$$H_2 - H_1 = P_2/\gamma_2 - P_1/\gamma_2 = \beta^2/2g\ (R_2^{\ 2} - R_1^{\ 2})$$

If $\gamma_1 = \gamma_2 = \gamma$, which is the case for most applications, where an incompressible fluid is used, then:

$$P_2 - P_1 = \gamma\beta^2/2g\ [R_2^{\ 2} - R_1^{\ 2}]$$

C. RADIALLY INFLOWING FLUID PASSING A ROTATING SMOOTH FACE

The prediction system for the radially inflowing fluid for a smooth impeller as indicated by this test program is given below. Because of the loss of a total pressure tap during one test of the smooth impeller configuration, the prediction method for this case is not considered as accurate as the methods for other cases that are reported herein.

The vortex exponent, n, is obtained from figure III-7 and the tangential fluid velocity at the impeller tip, Cu_o, from figure III-8. This information is then substituted into the general vortex equation,

$$(H_2 - H_1) = (P_2/\gamma_2 - P_1\gamma_1) = [(Cu_o\ R_o^{\ n})^2/2g(-n)]\ [R_2^{\ -2n} - R_1^{\ -2n}]$$

D. SHUTOFF FLOW FOR SMOOTH IMPELLERS

As demonstrated in the test program, a forced vortex exists in all cases where the pump is operating at shutoff flow or a flow coefficient of zero. The prediction method for this condition is the same as discussed in Section IV-B. The fluid velocity ratios can be found from figures III-4, or III-8, using $C_m/u = 0$.

E. BLADED DISK RADIALLY OUTWARD FLOW, RADIALLY INWARD FLOW, OR SHUTOFF FLOW

The radial pressure distribution along the bladed disk was found to obey the forced vortex theory if modified by a suitable constant, as follows:

$$(H_2 - H_1) = P_2/\gamma_2 - P_1/\gamma_1 = K^2\ \omega^{\ 2}/2g\ (R_2^{\ 2} - R_1^{\ 2})$$

The constant, K, was determined experimentally and found to be strongly dependent on radius, clearance, and blade height and to be little effected by flow coefficient from 0 to 0.02. The following equation was derived from a statistical fit of all of the test data obtained and reflects the dependence of K on T/S, R/Ro and T:

$$K = 0.951 - 0.282\ (R/Ro) + 0.2137\ (T/S) + 0.175\ (T).$$

The confidence in the effect of blade height, T, on the fluid velocity ratio, K, which is a linear function in the above equations, is low since it is based on only two values of blade height. Number of blades and direction of flow were found to have an insignificant effect, within the accuracy of the test data, and did not enter into the regression equation for K.

The calculation procedure for the pressure distribution using the forced vortex equation modified with K is a step-by-step calculation along the radius of the rotor surface. For example, the pressure rise between two radii, R_1 and R_2, would be calculated as follows.

1. Obtain from figures III-13, III-18, or III-21 a value of K based on the average radius between R_1 and R_2 and the particular T/S, T, and number of blades for the rotor.

2. Calculate $P_2 - P_1$ from the equation

$$P_2 - P_1 = \gamma K^2\ \omega^2/2g\ (R_2^2 - R_1^2)$$

The rotor should be divided into a number of small radial increments (e.g., $\Delta R^2 = 2$ in.^{2} works well), and $P_2 - P_1$ is calculated for each radial increment across the face of the rotor.

SECTION V
CONCLUSIONS

1. The "apparent" vortex modes for each of the disk configurations tested have been determined experimentally and are listed below.

   1. Smooth Disk - outward flow: forced vortex.
   2. Smooth Disk - inward flow: changing vortex depending on clearance, flow coefficient and radial span.
   3. Bladed Disk - inward or outward flow: changing vortex depending on radial span, axial clearance and blade height.

2. The pressure distribution for all of the bladed disks was found to be independent of flow direction (radially inward or outward), flow magnitude ($\phi = 0$ to $\phi = 0.02$), and slightly dependent on the number of blades (between 6 and 24).

3. For bladed disks and smooth disks with no through flow or radially outward flow, the pressure distribution has been shown to be predictable using the forced vortex equation modified by the experimentally derived constant K. K was found to be a function of axial clearance and flow coefficient for the smooth disk,

$$K = f(C_A, \phi) \text{ - (See figure III-4.)}$$

and for the bladed disk,

$$K = f(R/R_o, T/S, T) \text{ - (See figures III-13 and 18.)}$$

4. Determination of a pressure distribution prediction system for radially inward flow on a smooth disk has been found to be complex. Additional testing and analysis are required to obtain a more accurate description of the vortex mode for this case.

5. For the 24-blade impeller, blade height, T, and the ratio of blade height to axial clearance plus blade height, T/S, have a strong influence on torque coefficient, C_M. Reynolds numbers in the range of 4×10^6 to 2×10^7 have little influence on C_M except when the number of blades is small (six), in which case the effect is marked.

6. The high frequency pressure data showed that the peak-to-peak pressure amplitude across the blade of a rotating disk varies directly with the static pressure at each radial location and can be predicted by the following equation (within the range of the variables in this test program):

$$\Delta P = 0.074\ P_s.$$

7. A low frequency, relatively high amplitude pressure oscillation was observed across the bladed pumping surface. This was probably caused by recirculation flows disturbing the boundary layer on the casing, but will require further analysis to be definitely determined.

8. Back vane blade heights greater than 0.125 inch should be avoided in future centrifugal pump designs because of unstable recirculation flows and higher power consumed.

SECTION VI
REFERENCES

1. Stepanoff, A. J., "Leakage Loss and Axial Thrust in Centrifugal Pumps," ASME paper HYD-54-5, 1932.

2. Daily, J. W. and R. E. Nece, "Chamber Dimension Effects on Induced Flow and Frictional Resistance of Enclosed Rotating Disks," ASME Transactions, Journal of Basic Engineering, March 1960, pp 217-232.

3. Stepanoff, A. J. "Centrifugal and Axial-Flow Pumps, Wiley, New York New York, 1948.

4. Acosta, A. J. "Experimental and Theoretical Investigations of Two-Dimensional Centrifugal Pump Impellers," ASME Transactions, Vol. 76, 1954.

5. Schlichting, H., "Boundary Layer Theory," McGraw-Hill Book Co., New York, New York, February 1962.

6. Wood G. M., "Centrifugal Types of Dynamic Shaft Seals," ASME Paper 63-WA-167, 1963.

7. Maroti, L. A., G. Deak, and F. Kreith, "Flow Phenomena of Partially Enclosed Rotating Disk," Journal of Basic Engineering, ASME Transactions, September 1960.